New York City Panel on Climate Change 2018 Report Chapter 2: New Methods for Assessing Extreme Temperatures, Heavy Downpours, and Drought

J.E. González[1], L. Ortiz[1], B. K. Smith[2], N. Devineni[3], B. Colle[4], J. Booth[5], A. Ravindranath[2], L. Rivera[2], R. Horton[6], K. Towey[5], Y. Kushnir[6], and D. Manley[7]

[1] Mechanical Engineering Department & NOAA-CREST Center, The City College of New York, New York NY. [2] Department of Earth and Environmental Science, CUNY-Brooklyn College, New York, NY. [3] Civil and Environmental Engineering Department & NOAA-CREST Center, The City College of New York, New York NY. [4] School of Marine and Atmospheric Sciences of Stony Brook University, Stony Brook, NY. [5] Department of Earth and Atmospheric Sciences, The City College of New York, New York NY. [6] Lamont-Doherty Earth Observatory, Columbia University, Palisades, NY. [7]Columbia University Center for Climate Systems Research, New York, NY

Contents

2.1 Introduction

This New York City Panel on Climate Change (NPCC3) chapter builds on the projections developed by the second New York City of Climate Change Panel (NPCC2) (Horton *et al.* 2015). It confirms NPCC2 projections as those of record for the City of New York, presents new methodology related to climate extremes, and describes new methods for developing the next generation of climate projections for the New York metropolitan region. These may

This is the author manuscript accepted for publication and has undergone full peer review but has not been through the copyediting, typesetting, pagination and proofreading process, which may lead to differences between this version and the Version of Record. Please cite this article as doi: 10.1111/nyas.14007.

This article is protected by copyright. All rights reserved.

Author Manuscript

be used by New York City as it continues to develop flexible adaptation pathways to cope with climate change. The main topics of the climate sciences chapter are:

1. Comparison of observed temperature and precipitation trends to NPCC2 2015 projections;
2. New methodology for analysis of historical and future projections of heatwaves, humidity, and cold snaps, a new humidity variable;
3. Improved characterization of observed heavy downpours;
4. Improved characterization of observed drought;
5. Suggested methods for next-generation climate risk information.

The focus of NPCC3 is on high-risk events involving extreme temperatures, extreme precipitation, and drought. Current trends are presented using historical climate records of high temperature, cold snaps, humidity, and extreme precipitation for the New York Metropolitan Region. The geographical span of the New York Metropolitan Region considered here includes, in addition to New York City, adjacent sections of New Jersey such as Newark, Jersey City and Elizabeth, as well as other nearby locations in New York such as Yonkers and Long Island. Historical records of droughts in the Delaware watershed region are also examined. Each extreme climate variable is analyzed for current trends (a process known as detection), and future projections are updated for high temperature extremes as a test of new methods which can be utilized by NPCC4.

These new methods for next-generation projections that are suggested for use in NPCC4 are presented in appendices. These represent finer temporal and spatial resolutions that may be of practical use to key stakeholders in New York City for planning purposes and/or emergency responses. These include local projections of extreme heat and demonstrate the role of the heterogeneous landscape of the city in each process (i.e., how the urban heat island affects city neighborhoods differently). Each section of the chapter presents definitions, baselines, methods, and projections. Each section of the chapter closes with a section on uncertainties associated with the projections and recommendations for future work.

Box 2.1. Definitions and terms

Climate change

Climate change refers to a significant change in the state of the climate that can be identified from changes in the average state or the variability of weather and that persists for an extended time period, typically decades to centuries or longer. Climate change can refer to the effects of (1) persistent anthropogenic or human-caused changes in the composition of the atmosphere and/or land use, or (2) natural processes such as volcanic eruptions and Earth's orbital variations (IPCC, 2013).

Global climate models (GCMs)

Author Manuscript

This article is protected by copyright. All rights reserved.

A GCM is a mathematical representation of the behavior of the Earth's climate system over time that can be used to estimate the sensitivity of the climate system to changes in atmospheric concentrations of greenhouse gases (GHGs) and aerosols. Each model simulates physical exchanges among the ocean, atmosphere, land, and ice.

Representative concentration pathways (RCPs)

RCPs are sets of trajectories of concentrations of GHGs, aerosols, and land use changes developed for climate models as a basis for long-term and near-term climate-modeling experiments (Moss et al., 2010). RCPs describe different climate futures based on different amounts of climate forcings. These data are used as inputs to global climate models to project the effects of these drivers on future climate. The NPCC uses a set of global climate model simulations driven by two RCPs, known as 4.5 and 8.5, which had the maximum number of GCM simulations available from World Climate Research Programme/Program for Climate Model Diagnosis and Intercomparison (WCRP/PCMDI). RCP 4.5 and RCP 8.5 were selected to bound the range of anticipated GHG forcings at the global scale. RCP 4.5 is defined here as medium-emissions scenario, and RCP 8.5 is defined as a high-emissions scenario.

Climate change risk information

On the basis of the selection of the RCPs and GCM simulations, local climate change information is developed for key climate variables—temperature, precipitation, and associated extreme events. These results and projections reflect a range of potential outcomes for the New York metropolitan region.

Climate hazard

A climate hazard is a weather or climate state such as a heat wave, flood, high wind, heavy rain, ice, snow, and drought that can cause harm and damage to people, property, infrastructure, land, and ecosystems. Climate hazards can be expressed in quantified measures, such as flood height in feet, wind speed in miles per hour, and inches of rain, ice, or snowfall that are reached or exceeded in a given period of time.

Uncertainty

Uncertainty denotes a state of incomplete knowledge that results from lack of information, natural variability in the measured phenomenon, instrumental and modeling errors, and/or from disagreement about what is known or knowable (IPCC, 2013). See Box 2.2 for information on sources of uncertainty in climate projections.

2.2 General NPCC3 approach

As in NPCC2, NPCC3 makes use of definitions, measurements, baselines, and scenarios to represent how the probabilities of climate events may change in the future. Here the focus is on extreme events. For most climate hazards, the definitions of extremes are consistent with the NPCC2, specifically for extreme heat, cold spells and precipitation.

NPCC3 confirms the temperature and precipitation projections of NPCC2 as those of record that should be used for planning. Based on new and emerging science, NPCC3 introduces a new methodology for analyzing heat and precipitation extremes that could be used for developing future projections of record in NPCC4.

This article is protected by copyright. All rights reserved.

In NPCC2, temperature analyses included projections of average temperature changes and changes in heat waves and hot days. NPCC3 explores a new methodology for downscaling heat extremes and introduces new metrics to analyze historical and projected humidity. For precipitation, NPCC2 developed quantitative projections for average rainfall and daily maximum rainfall events, and NPCC3 introduces a methodology for quantifying projections for sub-daily heavy downpour rain events.

In addition to confirming NPCC2 projections as those of record for New York City, NPCC3 examined how current observations of temperature and precipitation changes compare to projected changes from NPCC2 into the 2020s time slice, which encompassed the time period from 2010 – 2039. Figure 2.1 shows the results of that analysis and demonstrates that observations from 2010 – 2017 – the period for which both observed data and NPCC2 projections are available to compare – have been largely consistent with projected changes in average conditions for both temperature (Fig. 2.1.a) and precipitation (Fig. 2.1.b). These comparisons should be viewed with caution because of the role that natural variation plays in the short term.

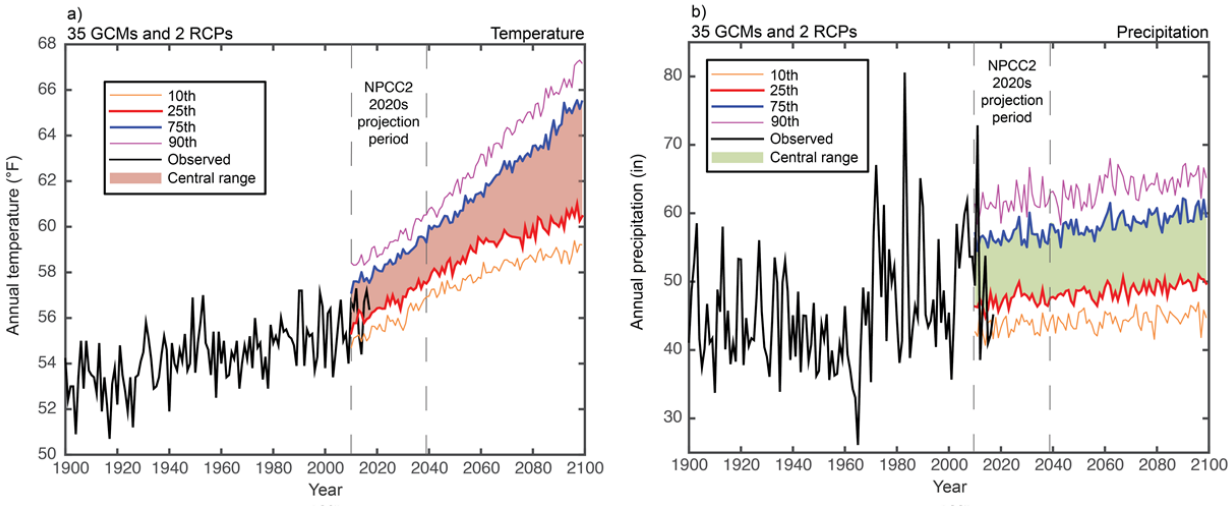

Figure 2.1. Observed and projected temperature changes compared with observations into the NPCC2 2020s (2010-2039) projected time slice for a) average annual temperature and b) average annual precipitation. Combined observed (black line) and projected (colored lines) average annual temperature (a) and average annual precipitation (b). Projected model changes through time are applied to the observed historical data. The colored lines represent the 10th, 25th, 75th, and 90th percentile of model projections across both RCP 4.5 and 8.5 for 35 GCMs. Shading shows the middle range of projections between the 25th and 75th percentiles. The vertical dotted line represents the range of the 2020s time slice from 2010 to 2039.

As NPCC3 shifts from a focus on average conditions to extremes, the baselines in some cases vary according to the relevance of the period for the extreme event researched

This article is protected by copyright. All rights reserved.

and the period for which data are available. To the extent possible, consistency with NPCC2 is maintained in this report. For example, the baseline for heat waves is 1971-2000, which is the same as NPCC2. However, NPCC3 uses summer months only for extreme heat events (June, July August) for three reference weather stations, while NPCC2 used the whole year with one reference weather station. NPCC3 uses bias-corrected statistical downscaling and develops future projections for extreme heat based on summer seasons only and includes high resolution dynamical downscaling at 1 km for selected time slices. Summer humidity is included in the projections as a new heat related variable. The section of extreme temperatures closes with a short view of cold spells or winter extremes. The section on urban flooding makes use of shorter, more detailed, records of satellite and radar data to demonstrate the spatial distribution of these extreme events at sub-hourly time resolution. For droughts, a much longer precipitation record is used to capture decadal variations across the Northeast, and tree-ring based streamflow reconstructions are used to understand how frequently extreme droughts have occurred in the past.

To create the new extreme event projections bias-corrected statistical downscaling is used (see Section 2.3). In an appendix, we provide an example of dynamic downscaling, a method that can capture the role of the urban built environment in magnifying heat events and mitigating flooding events. Here the role of the urban heat island in intensifying heat waves is addressed through comparing temperature statistics in New York City with nearby locations that are less urban.

Model outputs from the fifth phase of the Coupled Model Intercomparison Project (CMIP5) are used for projections of extreme heat. Methods for calculating future projections are consistent with NPCC2 but are updated consistent with the 2014 National Climate Assessment (Walsh et al. 2014) to account for the model biases in simulating the distribution of temperature. Results are provided in 30-year intervals centered on 2020, 2050, and 2080 as defined by NPCC2. The numerical ensemble of the CMIP5 considers multiple greenhouse gases scenarios, which better quantifies the uncertainties in these projections. See Box 1.2 in Chapter 1 for greater detail on uncertainties in climate change projections.

2.3. Extreme temperature and humidity

Summer (defined here as the months of June, July, and August) temperatures are expected to increase in New York City throughout the 21st century (Horton et al. 2015), leading to more frequent and intense extreme heat events known as heat waves. Here we follow the definition of heat waves according to the National Weather Service (NWS), i.e., an interval

Author Manuscript

This article is protected by copyright. All rights reserved.

of three (or more) consecutive days with temperatures of at least 90°F (32.22°C). Heat waves affect a wide range of human activities. These effects include increasing energy demand (Schaeffer et al. 2012; Sailor 2001; Santamouris 2014) and mortality (Knowlton et al. 2007; Luber and McGeehin 2008; Anderson and Bell 2010; Rosenthal et al. 2014). Moreover, higher temperatures associated with urbanization, a phenomenon called the urban heat island (UHI) (Oke 1982), exacerbate the impacts of extreme heat events (Li and Bou-Zeid 2013; Ramamurthy and Bou-Zeid 2016; Ramamurthy et al. 2017; Ortiz et al. 2018). New York City, being the most populated urban area in the United States with over 8 million people (US Census Bureau 2017), has a large human and economic incentive to understand and mitigate the negative impacts of these events now and in the future.

Extreme heat projections have primarily been developed on global (Meehl and Tebaldi 2004) or continental scales (Gao et al. 2012), with less work focusing on local urban projections that requires the accounting for fine-scale processes and feedbacks that may affect the occurrence and characteristics of high temperature events. An example of these processes is the soil moisture-heat wave feedback, wherein dry soil conditions may amplify heat waves by reducing available moisture for evaporative cooling (Seneviratne et al. 2006; Lorenz et al. 2010; Fischer et al. 2007). Cities may amplify these feedbacks by reducing exposed soil area, greatly reducing the capacity for water retention near the land surface (Li and Bou-Zeid 2013; Ramamurthy and Bou-Zeid 2016; Ramamurthy et al. 2017). Other relevant city-scale processes include waste heat from buildings and transportation (Taha 1997; Ichinose et al. 1999; Offerle et al. 2005), lower surface reflectivity of built surfaces (Taha et al. 1988; Morini et al. 2016; Ramamurthy et al. 2015) and increased heat storage in buildings and built structures (Oke et al. 1981; Arnfield and Grimmond 1998).

Humidity content of the atmosphere can play an adverse role in how humans react to high heat conditions (Davis et al. 2016; Hass et al. 2016). As air becomes more saturated with water vapor, the human body becomes less able to shed excess heat through evaporative cooling of perspiration. This can lead to exacerbation of high temperature impacts such as fatigue and heat exhaustion.

This section presents extreme heat and specific humidity projections for New York City using new methods, accounting where possible for urban effects via statistical processing of global climate model (GCM) simulation data. This statistical processing, or downscaling, is necessary because global models have, in general, very coarse spatial resolutions (> 100 km^2) and are thus not able to resolve fine details due to coastlines, topography, and land cover. The downscaling technique used here is named *histogram matching.* It aims to adjust the model representations of observed climate by correcting their *mean* and *variance* to match a representative set of observations in the target domain. This differs from the bias adjustment procedure of NPCC2 that combined GCM results with station records to downscale the projections to the New York Metropolitan Region using a method referred to as the “delta method” (Horton et al., 2015), where the projection ensemble is corrected

This article is protected by copyright. All rights reserved.

Author Manuscript

using the mean value from observations (for a detailed explanation of the difference between these methods see below, section 2.3.2.1).

Here in NPCC3, as in NPCC2, the climate projections are based on a multi-climate model ensemble, where each of the models was subjected to two Representative Concentration Pathways (RCP) scenarios – RCP4.5 (referred to as a medium-emissions scenario) and RCP8.5 (referred to as a high-emissions scenario) (see Box 2.1). The aim of this approach is to capture the uncertainties emerging from the range of model accuracy as well as those related to the impacts of future industrial activity, energy use policies and technology on the levels of greenhouse gas and aerosol emissions. For consistency, NPCC3 uses the same baseline period as the NPCC2 (1971-2000). Definitions and methods are detailed in Table 2.1 below.

Table 2.1. Definitions for heat extremes used in NPCC2 and NPCC3.

	NPCC2 (2015)	**NPCC3 (2018)**
Definition(s) of heat wave	• 3 or more consecutive days at or above 90°F	• 3 or more consecutive days at or above 90°F
Quantitative or Qualitative Measurement	Quantitative • Number of heat waves per year • Duration of heat wave (# days average heat wave lasts) • Total days above 90°F per year • Total days above 100°F per year	Quantitative • Number of heat waves per year • Duration of heat wave (# days average heat wave lasts) • Average maximum temperature during the heat wave (e.g., heat wave intensity) • Total days above 90°F per year • Total days above 100°F per year • Specific humidity ($kg_{vapor}/kg/_{air}$)
Baseline years	1971-2000	1971-2000
Baseline reference location	Central Park	Central Park (extreme heat) La Guardia Airport (extreme heat, humidity) JFK Airport (extreme heat)

Author Manuscript

This article is protected by copyright. All rights reserved.

Baseline value	• 2 heat waves per year • 4 days in duration	• 1.3 heat waves per year • 4 days in duration • 95.8°F maximum temperature • 11.1 days above 90°F • 0.28 days above 100°F • 0.0123 kg_vapor / kg_air
Future timeslices (# years and timeframes)	• 2020s (2011-2040) • 2050s (2041-2070) • 2080s (2071-2100)	• 2020s (2011-2040) • 2050s (2041-2070) • 2080s (2071-2100)
Methodology (RCPs, GCMs, percentiles, etc.)	• 2 RCPs (4.5 and 8.5) • 35 GCMs • 10^{th}, 25^{th}, 75^{th}, and 90^{th} percentiles across both RCPs and 35 GCM outputs • "Delta method" used for GCM bias correction	• 2 RCPs (4.5 and 8.5) • 26[1] GCMs • 10^{th}, 25^{th}, 75^{th}, and 90^{th} percentiles across both RCPs and 26 GCM outputs • GCM mean and variance bias correction with respect to temperature station records*.
Change metrics	• # heat waves per year • Duration of heat wave (# days average heat wave lasts)	• # heat waves per year • Average heat wave duration (# days) • Maximum temperature during the heat wave event • Annual Mean Specific Humidity
Results (Map, Table, other)	• Table of projected future values by percentile and timeslices	• Table of projected future values by percentile and timeslices • Time series of projected values with 95% confidence intervals

***** Bias correction is performed on GCM data in order to improve how representative a single grid box is to local New York City conditions. Details of these techniques are given in Appendix 2.C of this chapter.

[1] NPCC3 uses a smaller GCM ensemble than the 35-model ensemble used in NPCC2. This is due mostly to the fact that NPCC3 includes specific humidity and not all models provide such variable as standard output.

This article is protected by copyright. All rights reserved.

2.3.1 Observed trends in summer heat waves

Historical trends of daily maximum summer temperature in New York were analyzed using Central Park weather station, John F. Kennedy, and LaGuardia airports during June, July, and August (Figure 2.2). Central Park has the longest historical record, dating back to 1900, where the average annual daily maximum summer temperature trend has been rising at an average of 0.2°F per decade from 1900 to 2013. JFK and La Guardia weather stations go back to 1970, where average annual daily maximum summer temperatures have been increasing at a rate of 0.5°F per decade and 0.7°F per decade, respectively.

The distance between these weather stations provide insights into processes that affect temperatures near the surface, such as sea breezes[2] and the urban heat island. Sea breeze effects appear in stations located close to Long Island's southern shore (e.g., JFK), with lower daily maximum temperatures compared to their in-land counterparts (Figure 2.2). Sea-breeze impacts on temperatures show that geospatial heterogeneity of the urban landscape plays a role in near-surface temperatures, and therefore impact occurrences of extreme heat. The weather station located at JFK, which experiences afternoon sea breezes, has a mean summer maximum temperature of 80.6°F, whereas the other stations have a mean value of 82.7°F, which is 2.1°F higher. This is consistent with climatological studies (e.g., Gedzelman et al. 2003) of the urban heat island in the region, which have found that afternoon summer sea breezes may shift the center of the urban heat island west and north, towards New Jersey and The Bronx.

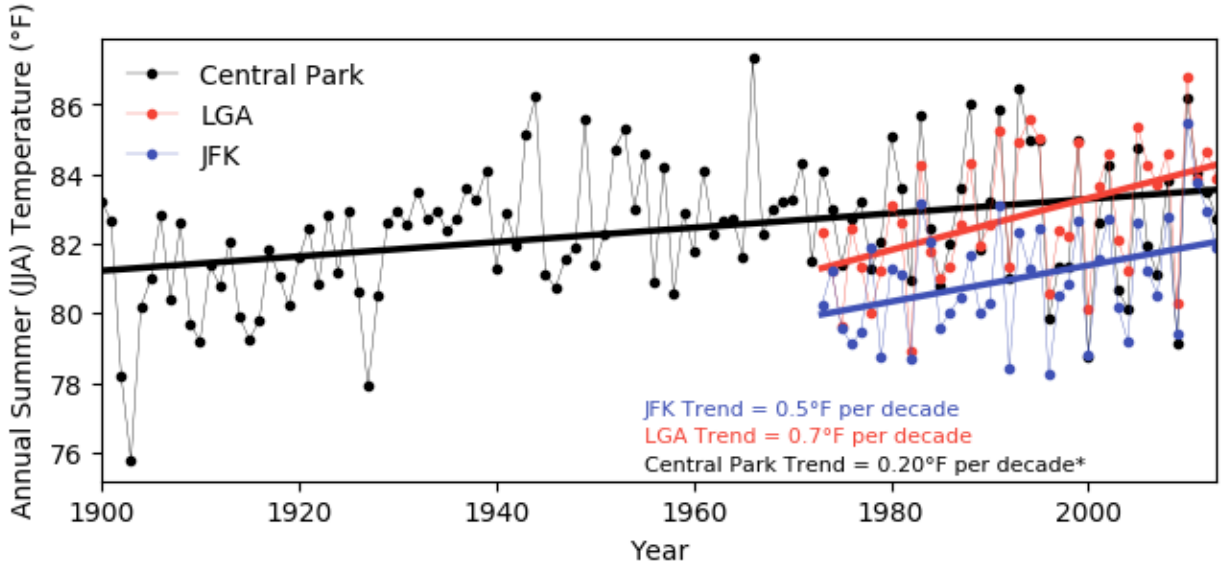

Figure 2.2. Observed annual daily summer maximum temperatures (June, July, August) in Central

[2] Sea breezes are a feature of the New York City southern coast (Childs and Raman 2005) and form due to temperature differences between the air over land and ocean (Haurwitz 1947).

This article is protected by copyright. All rights reserved.

Manuscript

Park from 1900 to 2013, LaGuardia (LGA) Airport from 1970 to 2013, and John F. Kennedy (JFK) airport from 1970 to 2013. Solid line represents linear trend in Central Park summer temperatures. Station records were obtained from the US Historical Climatological Network (USHCN) Version 2.5 (Menne et al., 2013). *Central Park trend is significant at 0.01 level, while LGA and JFK trends are positive but not significant possibly due to shorter record length.

2.3.2. New methods for projected changes in heat waves

This section describes new methods and results for NPCC3 projected changes in heat waves. Projections are presented in two formats:

- Graphical time series: Results shown as a time series are further broken out into the two RCP scenarios used in NPCC3 (see Fig. 2.3). These include a medium-emissions scenario (RCP4.5) (Thomson et al., 2011) and a high-emissions scenario (RCP8.5) (Riahi et al., 2011).
- Time slices table: Results are summarized for the 10^{th}, 25^{th}, 75^{th}, and 90^{th} percentile of model outcomes across both RCP 4.5 and 8.5 scenarios in Table 2.2, averaged by 30-year time slices centered around the 2020s (2010-2039), 2050s (2040-2069), and 2080s (2070-2099) decades.

2.3.2.1 Heat wave frequency, duration, and intensity

Heat wave characteristics considered here are their frequency (events/year), mean event duration (# days/event), and intensity (average maximum temperature/heatwave). NPCC2 had previously analyzed frequency and mean event duration; heat wave intensity is a new metric in NPCC3. While a new methodology is tested here that is different from NPCC2, NPCC3 confirms the use of NPCC2 projections as the projections of record for New York City to plan for extreme heat and suggests the consideration of new methodologies such as those presented here in NPCC3 for use in developing new projections of record in NPCC4.

Using a composite observed temperature record derived by averaging the daily maximum temperature over the three New York City stations, results from 26 GCMs were bias corrected in order to project distributions of heat waves for the NPCC3 time slices following the methods of Piani et al. (2010) and Hawkins et al. (2013) (See Appendix 2.A. for detailed methods). The bias correction method used belongs to the family of techniques named *histogram matching*, where statistics, in this case the mean and standard deviation, of a given variable are used to adjust the model distribution against the target observed distribution. For each GCM, the closest land grid point was selected, as was done in NPCC2, and the distribution of maximum daily temperature at this point was bias corrected against the City's composite maximum temperatures. This method is referred to here as a "single point" bias correction.

This article is protected by copyright. All rights reserved.

Author Manuscript

As indicated above, in NPCC2 the "delta method" was used to correct for the modes bias in representing the mean and variability of temperature in the target domain. This method, the average rise in each model's maximum temperature during each future 30-year time slice, compared to the baseline period, was calculated. This difference was added to the observed time series of daily maximum temperature at the reference station during the reference period, and the adjusted (higher) values were used to calculate the metrics described above (see Horton et al., 2015). Furthermore, NPCC2 used only one observational record, that of the station at Central Park. The previous NPCC2 approach may have resulted in a bias toward slightly cooler projected extreme temperatures compared to those projected using the NPCC3 bias-correction methods, particularly towards the warmer periods in the 2080s time slice. These changes may be due to the correction to the variance that, at least partially, addresses the fact that GCM grid boxes near coasts are over water.

NPCC3 analysis of the bias-corrected single point projections, show overall increase across all heat wave metrics throughout the 21st century (Fig. 2.3). To highlight the sensitivity to emission scenario we present in this figure the response to medium-emissions and high-emissions scenarios separately although in the summary, in Table 2.2, the projections are based on the multi-model distribution of model results showing the 10^{th}, 25^{th}, 75^{th}, and 90^{th} percentile outcomes across both RCP scenarios, as was done in NPCC2.

Mean daily maximum temperature (Fig. 2.3a) shows a nearly linear trend in the high emissions scenario (RCP8.5), whereas the rate of change in the medium-emissions scenario (RCP4.5) slows after 2040. The 95% confidence intervals become wider towards the latter half of the century, indicating greater uncertainty since they cover a spread of about 3°F, while the band is closer to 2°F in the first half.

The number of heat waves per year (Fig. 2.3b) shows far less deviation between the two emissions scenarios. Both scenarios increase at a pace of about 1 additional yearly event every 20 years until 2060, where growth slows down considerably. This may be due to consecutive events coalescing into very long heat waves, which becomes more likely as heat waves increase in length and frequency. It is also a side effect of the definition of heat wave used here, which establishes an unchanging temperature threshold through the entire century. As mean temperatures increase, meeting the 90 °F on consecutive days becomes more likely. Uncertainty in projections as described by confidence intervals increase over time, with a spread of 1 event in the first half of the century that grows to a spread of about 2 events by end of century.

Mean event duration projections (Fig. 2.3c) are similar across the scenarios in the first half of the century, growing by around 2 days per 20-year period. However, the high-emissions scenario projections show accelerated growth in the latter half of the century, as well as more spread in the model ensemble, with an uncertainty band spanning about 10 days, compared to about 2 days in the first half. This accelerated increase in event duration may explain the stabilization of event frequency projections in Figure 2.3b, as events may

This article is protected by copyright. All rights reserved.

Author Manuscript

aggregate into longer heat waves.

Mean intensity, defined as the mean of event maximum temperatures, shows large inter-annual variation (Fig. 2.3d), with projected values that increase from about 93 °F early in the century, to 95–98 °F by the end of the century. Confidence interval bands increase slightly throughout by end of century, reaching an ensemble spread of about 1 °F.

Author Manuscript

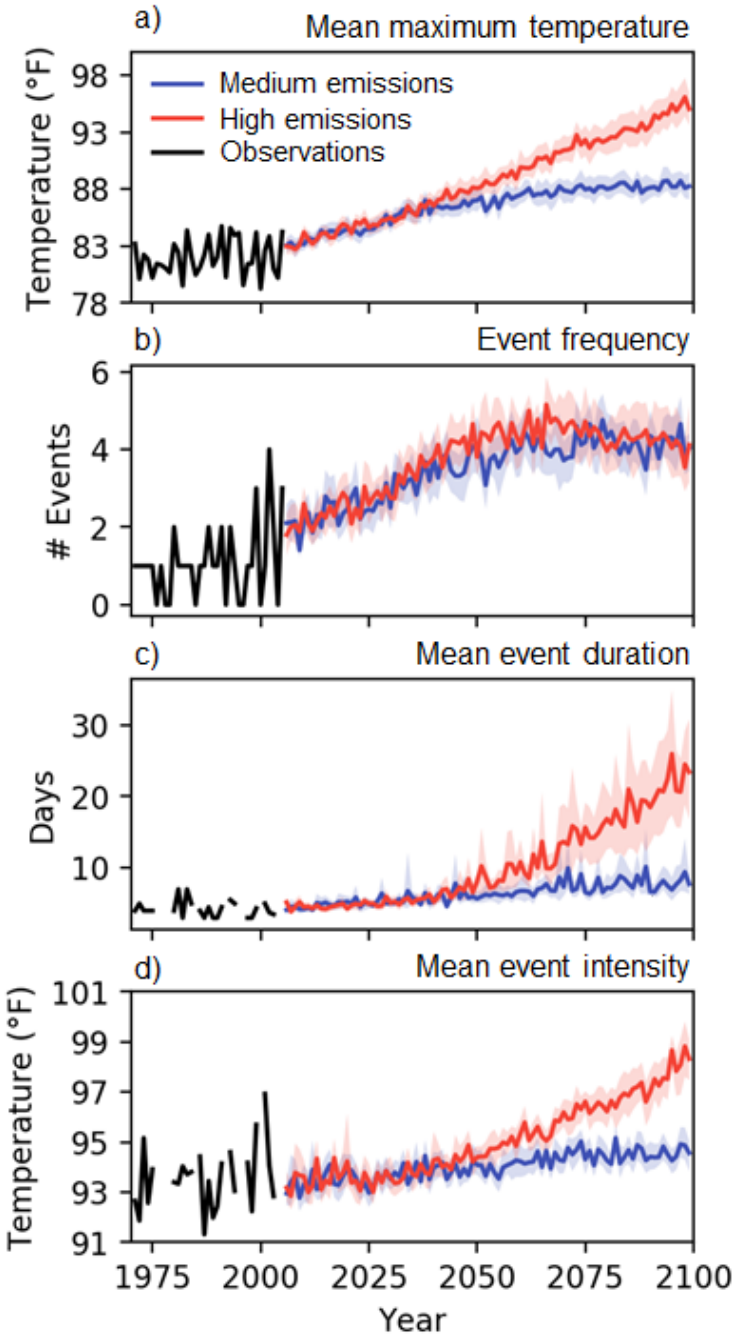

Figure 2.3. Results from new bias-corrected projections for future assessments of (a) mean daily maximum temperature, (b) event frequency, (c) mean event duration, and (d) mean event intensity compared to the 1971-2000 base period. Solid lines represent the multi-model mean of a 26 global climate model ensemble, while shaded bands show 95% confidence intervals. Black lines indicate

This article is protected by copyright. All rights reserved.

observations from three GHCN stations – Central Park, JFK, and LaGuardia – between 1971-2000.

Author Manuscript

2.3.2.2 New methods for warm day analyses

Additional key metrics of extreme heat explored are number of days above 90°F and 100°F in the summer season (Table 2.2). Projected days above 90°F (Table 2.2) are expected to become more likely as summer temperatures increase. By the 2080s, projections show increases ranging between 23 (10th percentile) to nearly 74 (90th percentile) times the 1971-2000 baseline[3]. Meanwhile, days above 100°F show increases in the 2080s of 0 (10th percentile) to 27 (90th percentile) times over the baseline period.

Heat wave and warm day projections are summarized in Table 2.2 across the entire ensemble of 26 model and 2 emissions scenarios as was done in NPCC2. Metrics are presented for 30-year time slices centered on the 2020s, 2050s, and 2080s decades. A one-to-one comparison with NPCC2 is also included for reference (where applicable) in Appendix 2.B. In general, the new projections point to about the same number of heat waves as NPCC2, however, with longer duration, and more days above 100^{o}F, in years between 75th and 90th percentiles. Projections for the first part of the century are close to those previously reported by NPCC2. The NPCC3 confirms the use of NPCC2 projections for days per year above 90^{o}F and 100^{o}F as those of projections of record for planning for the impacts of extreme heat.

Table 2.2. Results from new projection methods for future assessments of heat wave across 52-member ensemble (26 models, 2 projections) for New York City. Baseline refers to 1971-2000 average characteristics. See Appendix 2.B for comparison to NPCC 2015 projected values.

		Baseline	10th Percentile	25th Percentile	75th Percentile	90th Percentile
Heat waves per year *Average # events per year*	2020s	1.1	1	2	4	5
	2050s	1.1	2	3	5	6
	2080s	1.1	2	3	5	7
Mean heat wave duration *Average heat wave length in days*	2020s	4	3	4	6	8
	2050s	4	4	5	9	13
	2080s	4	4	6	15	27

[3] Although warm days can occur outside of the traditional summer months, here we only consider June, July, August, as extreme heat days are more likely to occur during this period.

This article is protected by copyright. All rights reserved.

Mean heat wave intensity *Maximum temperature during the heat wave event in °F*	2020s	97.4	91.8	92.5	94.5	95.7
	2050s	97.4	92.6	93.5	95.4	96.5
	2080s	97.4	93.2	94.2	97.1	99.1
Days above 90°F *Average # days per year*	2020s	9.6	6	11	25	34
	2050s	9.6	15	24	46	56
	2080s	9.6	23	34	62	74
Days above 100°F *Average # days per year*	2020s	0.27	0	0	0	2
	2050s	0.27	0	0	4	8
	2080s	0.27	0	1	13	27

Note: NPCC3 confirms the temperature projections of NPCC2 as those of record that should be used for planning. Based on new and emerging science, NPCC3 introduces a new methodology for analyzing heat extremes that could be used for developing future projections of record in NPCC4.

Author Manuscript

2.3.3 Methods for assessing trends in humidity

Humidity content of the atmosphere can play an adverse role in how humans react to high heat conditions (Davis et al. 2016; Hass et al. 2016). Here, we present projections of daily mean specific humidity based on a 26 multi-model ensemble, across medium and high emissions scenarios, as in section 2.3.2. For each model, the land grid point closest to New York City is used. Due to a lack of specific humidity records from all weather stations, GCM humidity was bias corrected based on La Guardia Airport only. In addition, the 1971-2000 baseline for specific humidity is based only on the La Guardia Airport weather station. Humidity is a new metric being considered by the NPCC3 and has not been addressed by previous NPCC reports.

Projections for summer periods (June 1 to August 31) show on average that increases in specific humidity by end of century tend to be larger on more humid days. Results show an increase between the 2020s and 2080s time slices of around 9% at each period's 10th percentile, while changes in the 90th percentile represent a 16% increase (Fig. 2.4). The uncertainty in these projections as characterized by the model ensemble 95% confidence bands (Fig. 2.4) are relatively large. Increases in specific humidity combined with increasing temperatures might lead to higher heat index (see Box 2.3), which has major

This article is protected by copyright. All rights reserved.

consequences for human health and is a driver of peak energy demand for space cooling, as air conditioning systems remove sensible (temperature-related) and latent (moisture related) heat from buildings. To fully assess combined air moisture and temperature impacts, concurrent values must be used, rather than the daily records found in the model ensemble. See Appendix 2.C of this chapter for an expanded discussion of how climate change is projected to impact the heat index. NPCC3 recommends further testing of this methodology for the development of new projections of record in NPCC4.

Box 2.3. Key humidity definitions

Specific humidity: A measure of the amount of water in the atmosphere, it is defined as the mass fraction of water vapor per unit mass of moist air.

Absolute humidity: Defined as the mass of air per unit volume of moist air.

Relative humidity: The ratio of water vapor pressure to the saturation vapor pressure. It measures how saturated with water vapor the atmosphere is. As air becomes more saturated with water vapor, it becomes more difficult for the human body to shed excess heat through evaporative cooling of perspiration.

Heat index: A measure of apparent temperature including the effects of temperature and relative humidity. It is defined in table format by the National Weather Service, although statistical approximations have been developed to approximate the heat index as a function of temperature and relative humidity.

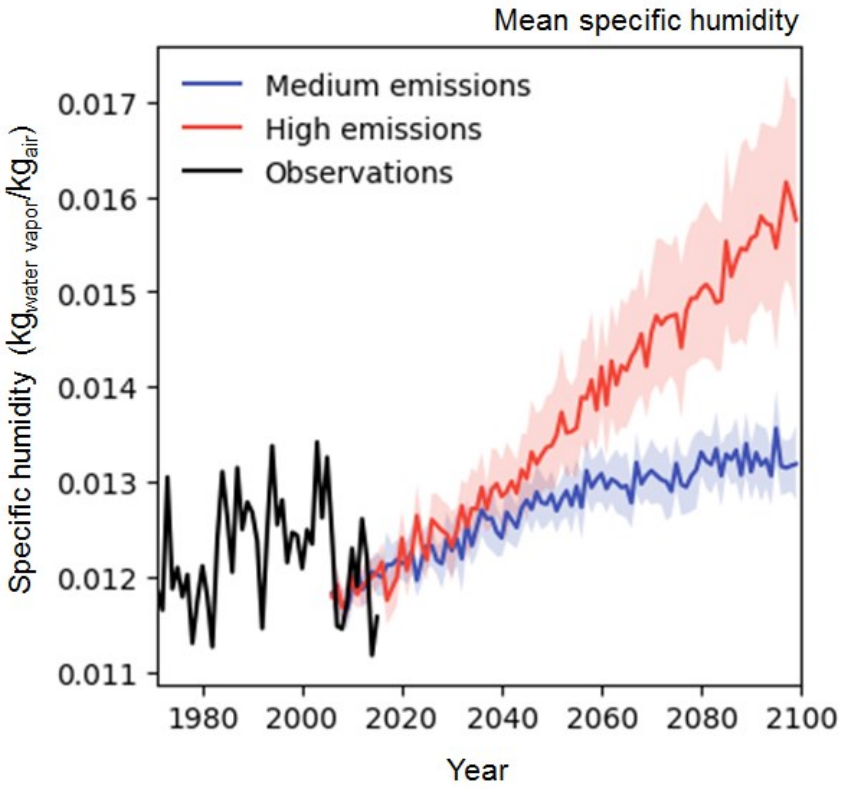

This article is protected by copyright. All rights reserved.

Figure 2.4. Specific humidity projections from the bias-corrected 26-member global climate model ensemble and across the medium (RCP4.5) and high (RCP8.5) emissions scenarios compared to the 1971-2000 baseline period at the La Guardia Airport weather station. Shaded bands represent 95% confidence intervals across the ensemble. Specific humidity refers to the amount of water vapor in the atmosphere and combined with increasing temperatures can lead to a higher heat index.

Table 2.3. Specific humidity projections across the 52-member ensemble (26 models, 2 projections) for New York City. Baseline period for humidity is 1971-2000 at the La Guardia Airport weather station.

		Baseline	10th Percentile	25th Percentile	75th Percentile	90th Percentile
Mean specific humidity (kg_{vapor}/ kg_{air})	2020s	0.0123	0.0115	0.0119	0.0127	0.0131
	2050s	0.0123	0.0122	0.0126	0.0138	0.0146
	2080s	0.0123	0.0125	0.0130	0.0149	0.0164

2.3.4. Cold snaps

NPCC3 confirms the analysis of NPCC2 days below 32°F as the projections of record for New York City Planning. NPCC3 further examines historical extreme cold events, using two measures of extreme cold (Boyle 1986; de Vries et al. 2012; Chen et al. 2016; Peterson et al. 2008; Efthymiadis et al. 2011):

- A *day below freezing* occurs whenever minimum temperature is equal to or less than 32°F
- A *cold day* occurs whenever its minimum temperature is equal to or less than the 10th percentile of daily minimum temperature of a given year.

Other definitions vary from these, including the use of standard deviations (Vavrus et al. 2006). Cold spell changes have been reported for regional scales (i.e. Europe; de Vries et al. 2012; China; Zhang et al. 2017; Northeast US; Thibeault and Seth, 2014) and for global scales (Vavrus et al. 2006) using GCMs ensembles and long-term climate records. In most cases, cold days have shown decreases, and more notable in Northern latitudes attributed to rapid melting of Arctic ice. It has been found that accelerated decreases of cold spells outpace increases in summer maxima (Thibeault and Seth, 2014).

We used Central Park Station to establish a benchmark for cold spells. The 10th percentile threshold for cold days at this station was computed from the entire 1900-2017 record, with a value of 24.08°F. In general, cold days per year decreased by 1.46 days every decade between 1900-2017, while days below freezing temperatures decreased at a rate of

This article is protected by copyright. All rights reserved.

Author Manuscript

1.85 days per decade (Figure 2.5). This results in recent years having, on average, about 22 fewer days below freezing and 17 fewer cold days than in 1900. These trends are slightly lower than those reported for the entire Northeast by Thibeault and Seth (2014). They report decreases of cold days of about 10 days from 1981-2010.

For the case of New York City, the attribution of these rapid decreases of cold spells may be a combined effect of global warming and urbanization. Urbanization leads to the urban heat island effect, which tends to have a larger effect the winter. NPCC2 provided projections of changes in number of days per year with minimum temperatures below 32°F and NPCC3 confirms those projections as projections of record.

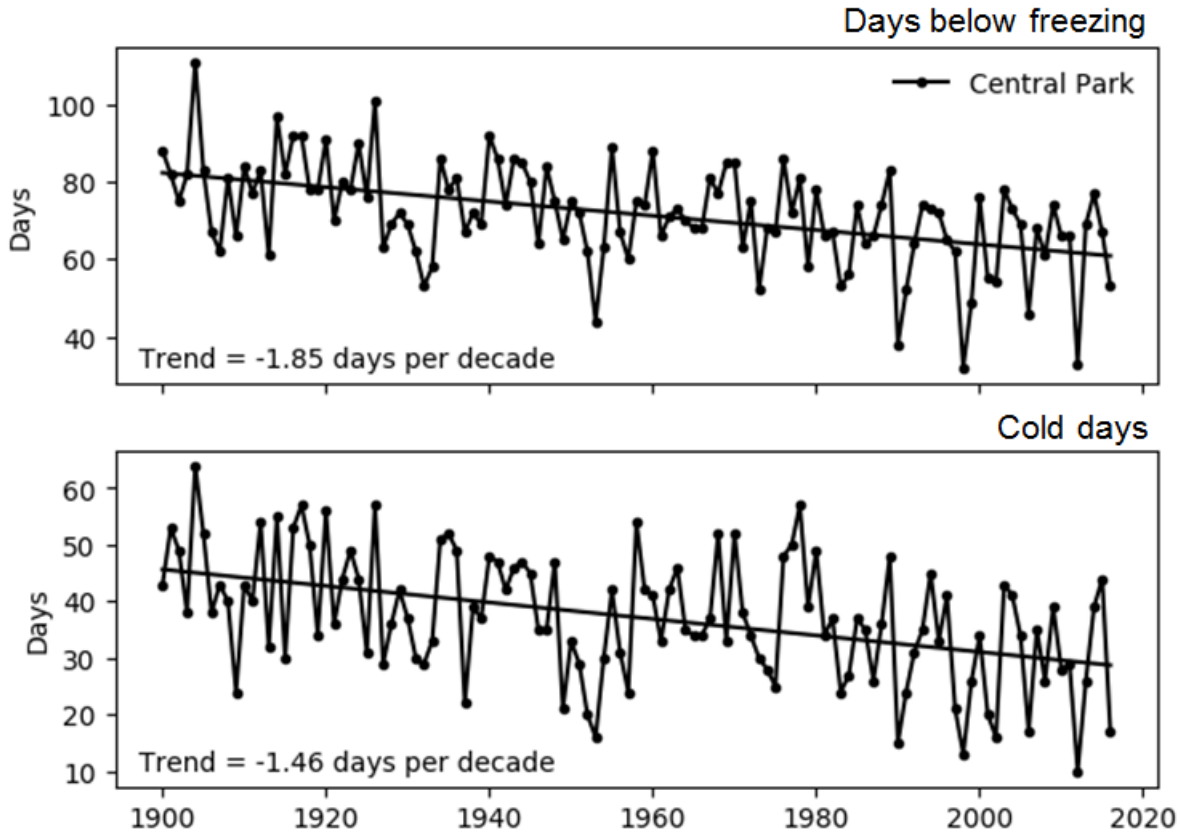

Figure 2.5. Observed annual cold days in Central Park Station (1900-2017). Solid straight lines represent the linear trend in days below freezing temperatures (top) and cold days (bottom). Station records obtained from the US Historical Climatological Network (USHCN). Both trends are significant at the 0.001 level.

2.3.5 Polar vortex and extreme cold events.

This article is protected by copyright. All rights reserved.

As indicated in the previous section, the impact of global warming on climate implies an overall decrease in the number of cold extremes while the number of warm extremes increase (Horton et al., 2015). However, recent persistent winter events of record cold weather in the Northeast US and in other Northern Hemisphere regions raised concern of a possible connection to climate change.

Both the science community (Screen et al., 2015) as well as the public (Lyond et al., 2018) have been engulfed in research and discussions of so-called “Polar Vortex” weather. An aspect of these discussions was the connection between the gradual disappearance of Arctic sea ice due to “Polar Amplification” and the increase in atmospheric “blocking” events, or the slowing-down and deepening of the wavy circulation in the mid-latitudes (Screen and Simmonds, 2010; Overland et al., 2015). With the increase in amplitude and slowdown of atmospheric waves, cold air can flow down from the Arctic deep into the mid-latitudes and vice versa, warm air flows north. This creates protracted deviations from normal conditions in either place.

This was the case in early January of 2014, when a large cold air mass moved from Canada into the northern Great Plains states and made its way slowly to the Northeast. The unusual cold weather in the eastern half of the US did not abate until April. At the same time, other areas in the Northern Hemisphere experienced record warm winter weather. Shorter events similar to this have happened since, as was the case during last (2017-2018) winter. The phenomenon was connected to so-called Stratospheric Warming, where the low-pressure vortex that is usually centered on the North Pole moves equatorward. This change in circulation in communicated down to the troposphere and results in anomalous weather situations during the season (Kretschmer et al., 2018; Screen et al., 2018).

There has been much debate whether such events are linked to the gradual melting of sea ice in the Arctic, and it appears that the answer is that there is a link (Overland et al., 2015; Screen et al., 2018). This was shown in climate models (Zhang et al., 2018) and is consistent with the observation that Polar Vortex events are on the rise (Kretschmer et al., 2018). There is, however, no evidence that extreme cold event in the U.S. have been on the rise as a result of this or other phenomena (Screen et al., 2015). Where the increase in Polar Vortex events was found to influence surface weather is in Siberia, where a significant cooling of the average winter weather has been detected, contrasting the observed warming elsewhere around the globe (Kretschmer et al., 2018; Zhang et al., 2018).

2.3.6 Summary and future research directions for extreme temperature and humidity

New methodologies for projections of heat wave characteristics for the New York Metropolitan Region were tested in NPCC3 using bias corrected climate model projections.

This article is protected by copyright. All rights reserved.

Author Manuscript

For the early part of the century (2020s), these updated projections are consistent with those of NPCC2. In the later part of the century (2050s and 2080s), however, the NPCC3 projections presented in this chapter display more intense heat events with longer durations. This is because the new projections correct for the under-estimation of the extreme temperatures simulated for the region in the GCMs in the current climate.

Projections show large changes across all heat wave metrics throughout the 21st century. The high emissions scenario (RCP8.5) projects, in many cases, several times larger effects than medium-emissions scenario. The uncertainty of the projections increases through time. The new NPCC3 projections include humidity, which is projected to increase by more than 30% from present benchmarks. These increases in atmospheric humidity with extreme temperatures are likely to have large societal implications reflected in public health and energy demands.

NPCC3 confirms the NPCC2 projections for heat waves, hot days, and cold days as those of record for New York City in planning for the impacts of climate change and recommends the incorporation of this newer methodology into revised projections of record in NPCC4. Future work in projecting extreme heat and humidity for the NPCC should be directed to incorporating the spatial distribution of these extreme heat events to account for coastal influence and urban heat island effects (e.g., sea-breeze effects). This will require dynamic downscaling using regional climate models (RCMs) to dynamically downscale climate projections to finer spatial scales within the New York Metropolitan Region. Carrying this out for an ensemble of GCMs and RCMs will require large computational efforts. New methods may be needed to account for uncertainties in dynamic downscaling. See Appendix 2.D for an example of the possible approach utilizing one GCM and one RCM, for two time slices, the middle and end of the century, as a potential guide for new research directions in NPCC4.

2.4. Heavy downpours and urban flooding

NPCC2 projected quantitative changes in daily extreme rainfall amounts for 1 inch, 2 inches, and 4 inches (Table 2.4). NPCC2 also included a qualitative projection in relation to extreme rainfall, stating that heavy downpours in the New York Metropolitan Region are very likely to increase by the 2080s (Horton *et al*., 2015).

NPCC3 does not provide new projections for heavy rainfall and confirms the NPCC2 projections as those of record for City planning and adaptation. NPCC3 provides new analysis and a deeper dive into understanding the dynamics of heavy rainfall events in the New York Metropolitan Region that set the stage for recommended use of developing new projections of record in NPCC4.

This article is protected by copyright. All rights reserved.

Author Manuscript

NPCC3 focuses on observed annual rainfall (see Section 2.2) and observed heavy rainfall days in recent years compared to the NPCC2 2020s time slice projections. NPCC3 also focuses on the types of storm systems associated with heavy rainfall events, and the regional drivers of historical flash flooding events. This section also looks at a trend analysis of sub-daily heavy precipitation events at the 1-, 3-, 6-, and 24-hour duration. Finally, this section explores ways to illustrate the spatial variation of urban flooding events. It is recommended that this work serve as a foundation for new projections of record for heavy rainfall that are to be developed in NPCC4.

Manuscript

Table 2.4. NPCC2 projected changes in heavy rainfall days (Horton *et al.*, 2015). Projections are based on 35 GCMs and 2 RCPs. Baseline data are for the 1971-2000 base period. Projections show the low estimate (10th percentile), middle range (25th to 75th percentile), and high estimate (90th percentile) 30-year mean values from model-based outcomes. NPCC3 confirms the use of these NPCC2 projections as those of record for City policy and planning purposes.

Heavy Rainfall Days	Baseline (1971-2000)	Low estimate (10th percentile)	Middle range (25th to 75th percentile)	High estimate (90th percentile)
2020s				
# days rainfall ≥ 1 inch	13	13	14-15	16
# days rainfall ≥ 2 inches	3	3	3-4	5
# days rainfall ≥ 4 inches	0.3	0.2	0.3-0.4	0.5
2050s				
# days rainfall ≥ 1 inch	13	13	14-16	17
# days rainfall ≥ 2 inches	3	3	4-4	5
# days rainfall ≥ 4 inches	0.3	0.3	0.3-0.4	0.5
2080s				
# days rainfall ≥ 1 inch	13	14	15-17	18
# days rainfall	3	3	4-5	5

This article is protected by copyright. All rights reserved.

≥ 2 inches				
# days rainfall ≥ 4 inches	0.3	0.2	0.3-0.5	0.7

Note: Like all climate projections, the NPCC climate projections have uncertainty embedded within them. Sources of uncertainty include data modeling constraints, the random nature of some parts of the climate system, and limited understanding of some physical processes. The NPCC characterizes levels of uncertainty using state-of-the-art climate models, multiple scenarios of future greenhouse gas concentrations, and recent peer-reviewed literature. Even so, the projections are not true probabilities and the potential for error should be acknowledged.

NPCC3 analyses of heavy downpours build on NPCC2 projections for daily extreme rainfall by more closely examining the past and present rainfall across New York City and across timescales. Additionally, NPCC3 includes analyses of urban flooding (definition in Table 2.3), past and present, in New York City and surrounding areas. NPCC3 refocuses discussion from daily extreme rainfall to sub-daily 'heavy downpours' defined as rarely occurring rainfall at less-than daily timescales that can produce urban flooding. NPCC3 lays the groundwork for a new set of future projections in NPCC4 using these new metrics. Definitions of rainfall and urban flooding terms included in NPCC3 are in Table 2.5.

Table 2.5. NPCC3 rainfall and urban flooding definitions.

Term	Definition
Daily extreme rainfall	Rainfall depths at the far end of the rainfall probability distribution. Extreme rainfall is defined as the number of days per year which exceed 1, 2, and 4 inches of rainfall averaged across New York City (as in NPCC2)
Heavy downpours	Rainfall at the 1-hr, 3-hr, 6-hr, and 24-hr durations which may cause urban flooding. For statistical analyses, the annual maximum values are used. These heavy rainfall intensities may differ across New York City rain gauges.
Days of known flooding	Urban flooding identified by experts (emergency managers and National Weather Service) through either the New York City Hazard Mitigation Reports or the National Climactic Data Center Storm Events Database.
Urban flooding	Surface flooding of an urban (generally over 20% impervious) area. Urban flooding is caused by rain falling faster than local conveyance systems (sewers or streams) can transmit it. When available, streamflow data from small urban streams in the New York City metropolitan region is used as a proxy for New York City urban flooding datasets.

Extreme rainfall is defined as a rainfall amount that is a rare event, i.e., one that approaches the end of the probability distribution of all events. In NPCC2, daily extreme rainfall in the current climate was represented by the number of occurrences of rainfall

This article is protected by copyright. All rights reserved.

Author Manuscript

above 1, 2, or 4 inches per day at the Central Park weather station in New York City. Extreme rainfall measured at Central Park has significant year-to-year variation such that no statistically significant trends in extreme rainfall can be identified (Horton et al. 2015). A statistically significant trend indicates that this trend in extreme rainfall would be unlikely to occur by chance. NPCC2 did note that the heaviest 1% of daily rainfalls have increased by approximately 70% between 1958 and 2011 in the Northeast (Horton et al., 2015). NPCC2 used the observed measurements as a baseline for projections of extreme rainfall (Table 2.6 (NPCC2, 2015)).

Table 2.6. NPCC2 Daily Extreme Rainfall Analyses (from Horton et al., 2015)

Extreme precipitation	**NPCC2 (2015)**
Definition(s)	• Individual days per year with rainfall at or above 1 inch • Individual days per year with rainfall at or above 2 inches • Individual days per year with rainfall at or above 4 inches
Quantitative or qualitative measurement	Quantitative • # days per year with rainfall reaching at or above daily rainfall total
Baseline years	1971-2000
Baseline value	• 13 days (1 inch) • 3 days (2 inches) • 0.3 days (4 inches)
Future time slices (# years and timeframes)	30-year time slices for • 2020s (2011-2040) • 2050s (2041-2070) • 2080s (2071-2100)
Methodology (RCPs, GCMs, percentiles, etc.)	• 2 RCPs (4.5 and 8.5) • 35 GCMs • 10^{th}, 25^{th}, 75^{th}, and 90^{th} percentiles across both RCPs and 35 GCM outputs
Change factor	• # days per year reaching daily rainfall threshold
Results (Map, Table, other)	• Table of projected future values by percentile

This article is protected by copyright. All rights reserved.

2.4.1 Extreme Rainfall and Heavy Downpours

This section focuses on extreme rainfall analyses by describing the approaches to heavy downpours in NPCC2 and NPCC3, describing regional drivers of daily and sub-daily heavy rainfall, providing a revised historical analysis of heavy rainfall across New York City, and summarizing new research projecting changes in heavy downpours in the region.

2.4.1.1 Extreme daily rainfall and links to tropical and extratropical cyclones

NPCC2 results included projections for extreme rainfall in the 2020s (2010-2039), 2050s (2040-2069), and 2080s (2070-2099) compared to the baseline (1971-2000) at Central Park. Data for the first eight years of the 2020s time-slice can now be compared to projections – as has been done above with climate averages in Section 2.2. However, several caveats should be kept in mind. First, the fewer years of data, the more likely that year-to-year variations will outweigh any longer-term climatic trends in data. Second, if there is a substantial climatic trend in rainfall extremes, the first eight years of a 30-year time slice may look substantially different than the last eight years of the time slice. Table 2.7 shows the 2020s (defined as 2011-2040) extreme daily rainfall projections from NPCC2 compared to actual rainfall data from 2011-2017 and the baseline values from 1970-2003. The first observed 8 years of the 2020s time slice show that observed heavy daily rainfall totals have fallen within the low- to middle-range estimate of the projected amounts.

Table 2.7. Comparison of NPCC2 daily extreme rainfall projections for the 2020s time slice (2010-2039) to observed values at Central Park (2011-2017) and baseline values (1971-2003).

Heavy rainfall days	Baseline values (1971-2000)	NPCC2 2020s low estimate (10^{th} percentile)	NPCC2 2020s middle range (25^{th}- 75^{th} percentile)	NPCC2 2020s high estimate (90^{th} percentile)	Observed values (2011-2017)
# days ≥ 1 inch	13	13	14-15	16	14.1
# days ≥ 2 inches	3	3	3-4	5	2.7
# days ≥ 4 inches	0.3	0.2	0.3-0.4	0.5	0.4

Projections of extreme rainfall at the daily scale were analyzed in detail in the NPCC2 Report. Therefore, NPCC3 confirms NPCC2 as projections of record, and aims to provide supplemental information by providing a benchmark analysis on the seasonal characteristics

This article is protected by copyright. All rights reserved.

Author Manuscript

governing daily precipitation extremes in the recent historical record, as well as provide an overview of recent studies of precipitation extremes that have occurred since NPCC2.

The primary large weather systems that affect New York City are cyclones. Cyclones refer to low pressure regions where air converges and causes uplift. Cyclones can include extratropical cyclones, caused by mid-latitude weather fronts (for example, Nor'Easters) and tropical cyclones, which originate in the tropical oceans (for example, hurricanes). Tropical cyclones are tracked for weather forecasts and extratropical cyclones can be tracked semi-objectively. The tracks for both types of cyclones are used to associate extreme precipitation with storms.

The precipitation data used in this section is daily weather station data from John F. Kennedy, LaGuardia, and Newark International airports available from the Integrated Surface Database (Smith et al. 2011). The extremes are defined as 24-hr precipitation for the top 1% of days for the record, per station, which translates to 138 days per site. The baseline period used, 1979 – 2016, was selected based on the availability of satellite-era gridded sea level pressure (SLP) reanalysis data (Dee et al., 2011) at the time of preparation of this analysis. SLP fields are used to track extratropical cyclone centers, via the numerical algorithm of Bauer et al. (2016). Cyclone association is calculated by checking if a cyclone center is within 1000 km of New York City on the date of the precipitation event. However, all cyclones that ended up being associated with a precipitation extreme passed within 500 km of New York City. Additional details of the analysis method are in Towey et al. (2018).

Daily (24-hr) precipitation extremes during the 1979 – 2016 period occurred most often in August, but more than one event occurred in each month of the year. For events in winter months, the precipitation most likely fell as snow, but the snow-water equivalent is used for this analysis. Figure 2.6 summarizes annual cycle for extreme 24-hr precipitation events. Extratropical cyclones cause the larger number of extreme 24-hr precipitation events in each month of the year. Tropical cyclone and non-cyclone events tend to occur in summer and early fall. Other events may simply be related to small-scale storms with no mesoscale organization. These types of storms are likely to drop all their precipitation in a short time period and be associated with shorter-term heavy rainfall. They are the focus of the remainder of this section. For a more detailed analysis of extreme rainfall and cyclones, see Appendix 2.E.

Author Manuscript

This article is protected by copyright. All rights reserved.

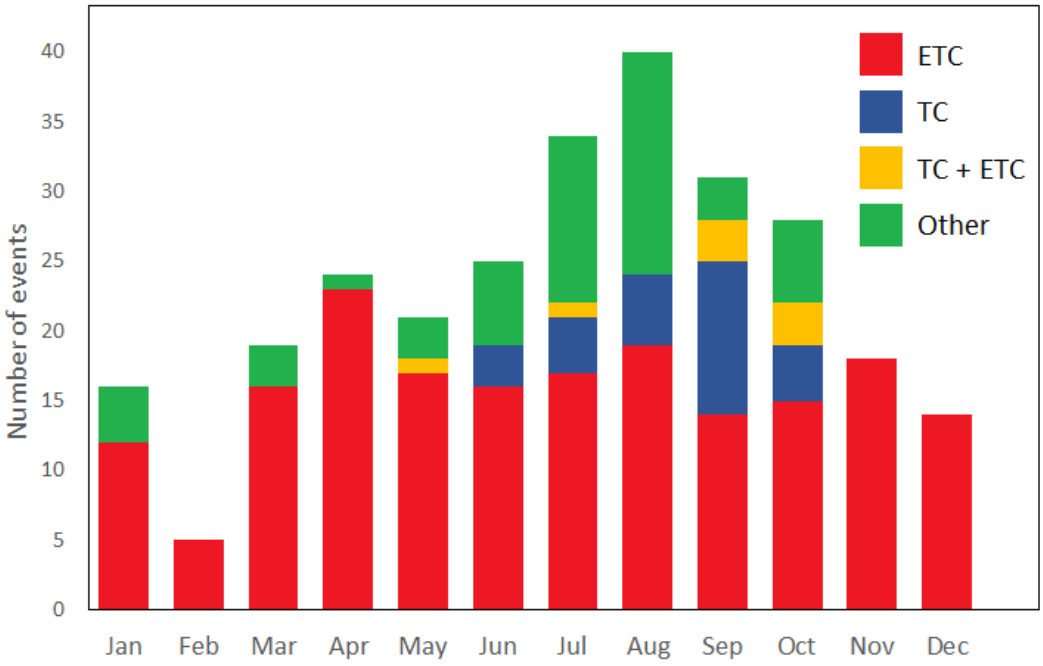

Figure 2.6. Total number of extreme 24-hr precipitation events at three New York City airports (JFK, La Guardia, and Newark) per month from 1979-2016 correlated with storm type. Color indicates the storm type. If more than one airport measured a precipitation extreme on the same date, then that event is only counted once in this figure. ETC refers to extra-tropical cyclones and TC to tropical cyclones; TC+ETC are hybrid storms that display characteristics of both types. Cyclones are identified using Modeling, Analysis, and Prediction (MAP) Climatology of Midlatitude Storm Area (MCMS; Bauer et al. 2016). Tropical cyclones are distinguished by the presence of HURicane DATabase tracks. Note: 'Other' refers to events outside of tropical and extratropical cyclone events that may be related to small-scale storms with no mesoscale organization.

Author Version

2.4.1.2 Regional outlook on heavy rainfall at sub-daily scales

Building upon the daily rainfall extremes analysis in NPCC2, NPCC3 also examines methods to examine heavy downpours that often drive urban flooding, looking at sub-daily events at occurring at one- to six-hour timescales (Smith et al. 2013). Rainfall that drives urban and flash flooding in the Northeast is typically temporally and spatially concentrated and is most often caused by thunderstorms (Figure 2.7) (Smith and Smith 2015). Regarding projections, NPCC2 included a qualitative projection that downpours are "very likely" to increase by the 2080s. NPCC3 does not update this prediction but does establish heavy downpours as an additional quantitative variable to be included in projections in NPCC4.

Since NPCC2 there have been a few new studies using global climate model projections of precipitation extremes in the Northeast US. The results from these studies are consistent with the NPCC2 Report in that they project an increase in precipitation, both in terms of the mean and extremes for the region (Ning et al., 2015). These precipitation changes are expected to occur in both winter and summer seasons (Fan et al. 2014).

This article is protected by copyright. All rights reserved.

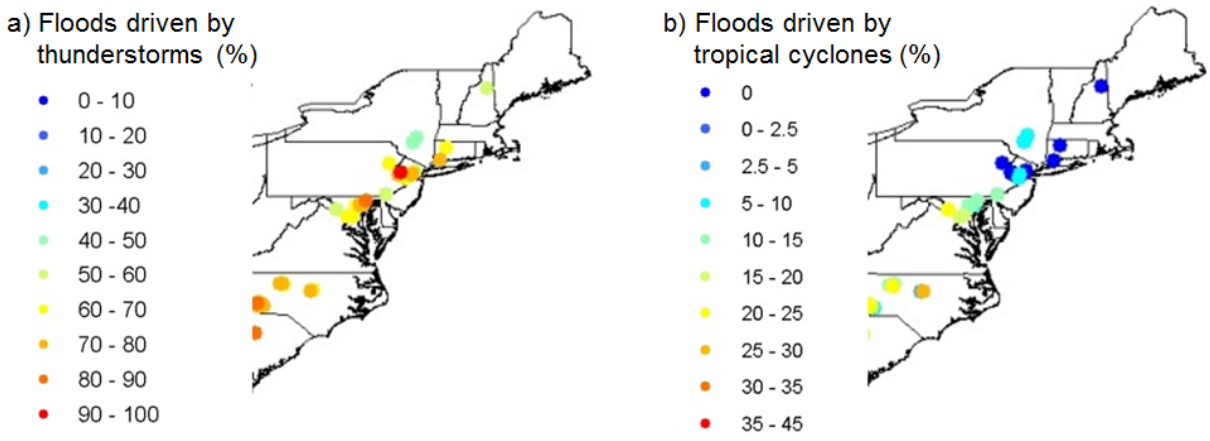

Figure 2.7. Proportion of flash flood events (streamflow > 92 $ft^3\ s^{-1}mi^{-2}$ or $1m^3\ s^{-1}km^{-2}$) on small (<5.8 mi^2 or 15 km^2) USGS gauged streams in the Northeastern US caused by a. thunderstorms and b. tropical cyclones. (Adapted from Smith and Smith 2015). Thunderstorms are distinguished by the presence of lightning flashes, while tropical cyclones are distinguished by the presence of HURicane DATabase tracks. Data are for the entire period of record for each stream gauge, generally from the mid-1980's to 2015.

Author Manuscript

However, the uncertainty in these precipitation projections is much larger than the uncertainty in the modeled temperature projections. One reason for the uncertainty is the presence of modes of natural variability, such as the North Atlantic Oscillation[4], that affect precipitation in the New York Metropolitan Region. These can have strong inter-annual impacts on the location and the types of cyclones that generate at least half of the strong precipitation events for the region (see e.g., Hall and Booth, 2017). Additionally, the issue of characterizing and projecting Northeast US precipitation extremes and their relationship to natural climate variability has been found to be more complicated than understanding the cyclone tracks (Ning and Bradley, 2014).

A recent study from Castellano and DeGaetano (2015; 2017) has projected future rainfall intensity-duration-frequency (IDF) curves for New York State. These project future rainfall extremes for durations longer than one hour using a set of downscaled global and regional climate models (Castellano and DeGaetano 2015; DeGaetano and Castellano 2017; Castellano and DeGaetano 2017). Future IDF curves were developed by using change factors calculated as change in rainfall between past observations and downscaled climate model projections of future rainfall. These projections, which can be found online at http://ny-idf-projections.nrcc.cornell.edu/, are more certain for rainfall durations of more than 24-hours

[4] The North Atlantic Oscillation, or NAO, is a fluctuation in sea level atmospheric pressure between the Icelandic Low and Azores High. It influences the climate pattern in the Northern Hemisphere.

This article is protected by copyright. All rights reserved.

than for those under 24-hours (DeGaetano and Castellano 2017). Regardless, these are the only peer-reviewed, local, sub-daily rainfall projections available for New York City, and are used in development of the New York City Climate Resiliency Design Guidelines (http://www1.nyc.gov/assets/orr/pdf/NYC_Climate_Resiliency_Design_Guidelines_v2-0.pdf).

2.4.1.3 Heavy downpours past trends and baselines

For NPCC3, historical trends in heavy downpours were analyzed using hourly data from multiple New York City-area NOAA rain gauges at Central Park, LaGuardia Airport, John F Kennedy Airport, and Newark Airport. This analysis allows for an investigation of trends in short-duration heavy downpours. Heavy downpours, defined as the annual maximum hourly, 3-hourly, 6-hourly, and daily rainfall depth were analyzed for change points. Change points indicate that the median rainfall depth has changed in that year, while trends indicate a gradual and continuous shift in medians throughout the time-period (see Figure 2.8 for examples). Methods for determining trends in extreme rainfall included the nonparametric Pettitt Test (Pettitt, 1979), nonparametric Mann-Kendall Test (Mann, 1945; Kendall, 1975), and Sen's Slope (Sen, 1968).

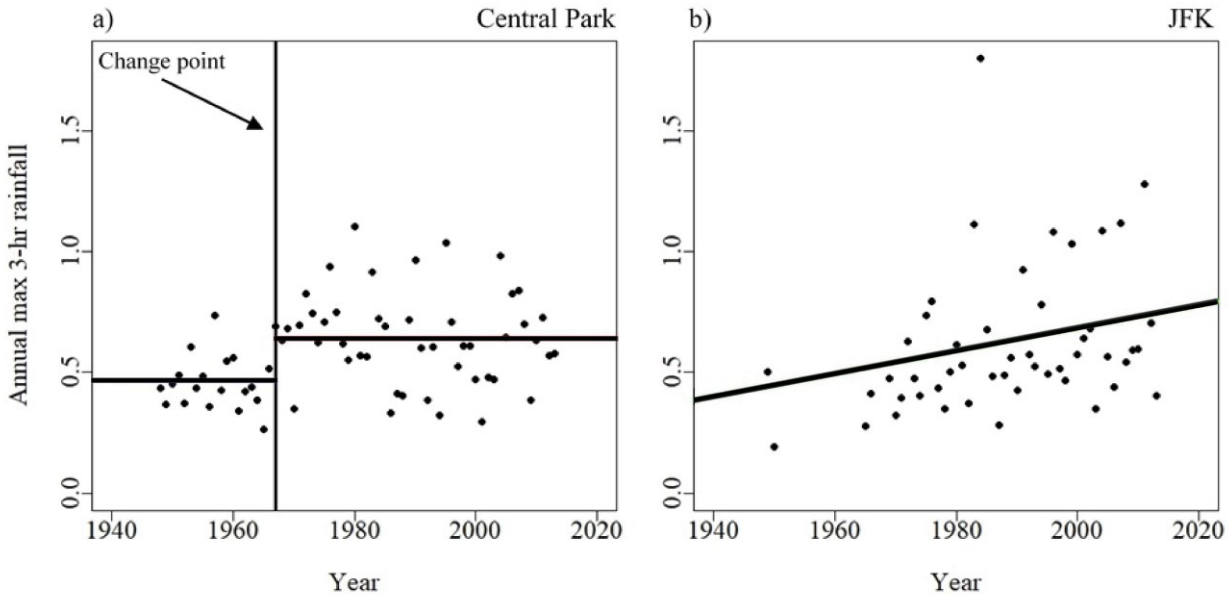

Figure 2.8. Annual maximum rainfall at Central Park (a) and JFK (b) rain gauges. Central Park displays a change point, a change in median rainfall depth, in 1967 (vertical line) and JFK displays an increasing trend.

This article is protected by copyright. All rights reserved.

Historic trends in heavy downpours are difficult to establish. The natural annual variation in rainfall maxima are generally more significant than trends over time, so that few statistically significant change-points or trends can be found in the rainfall record (see Appendix 2.E for specific results). Statistical results indicate that change points can be detected at the Central Park rain gauge in the mid-1960s at the 3- to 24-hour timescale for annual maximum rainfall. Change points can also be detected at the Newark Airport rain gauge in 1971 for 1-hour and 24-hour annual maximum rainfall. These change points may represent a meteorological regime shift associated with the wetter years after the mid-1960s drought, or they may represent changes in recording. After accounting for change points, few rainfall records exhibit statistically significant trends in annual maxima. The only significant trend is for the 3-hour annual maximum rainfall depth at the John F Kennedy Airport rain gauge (Fig. 2.8). Across rain gauges and time-scales, it appears that there may have been an upward shift in extreme rainfall in the late 1960s to early 1970s, but that there has been no consistent trend in heavy downpours across the city.

In order to define current baseline and spatial variation for heavy downpours in New York City, a high-resolution rainfall dataset for 1 km^2 and 15-minute intervals was developed using warm season rainfall from 2001-2015 for the Fort Dix, NJ (KDIX) SR-88D (Weather Surveillance Radar, 1988 Doppler) radar in Mount Holly, New Jersey operated by the National Weather Service (See Appendix 2.E for details of methods).

Baseline data for heavy downpours in New York City indicate a spatial variation in rainfall depth (Fig. 2.9). Days of known flooding (from Hazard Mitigation Reports and NCDC) vary in rainfall depth between 0.9 to 1.25 inches across New York City. Rainfall on flooding days is at a maximum (1.25 in) over the geographic center of the city (North Brooklyn and Southeast Queens), while some areas of high rainfall extend downwind of the city to the northeast. This region of high rainfall rates can be related to the urban impact on convective rainfall with higher rainfall within the city center and downwind (northeast). The impact of the Long Island Sound in decreasing rainfall can be seen in the rainfall map with lower rainfall over the sound. An important finding is that relatively low rain rates can cause flooding in New York City (Fig. 2.10).

Author Manuscript

This article is protected by copyright. All rights reserved.

Manuscript

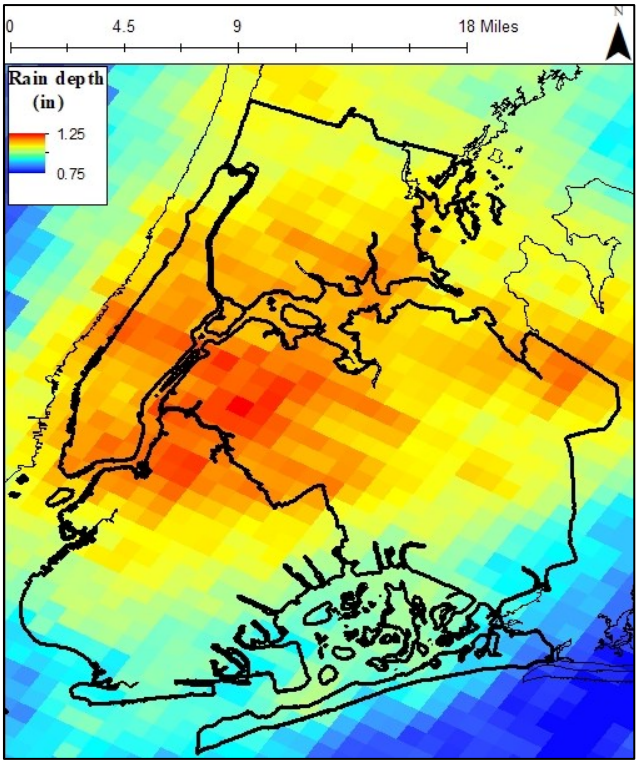

Figure 2.9. Daily average rainfall for days of known flooding (2001-2015). Rainfall data from Staten Island are missing due to a blocked radar band. Image adapted from (Smith and Rodriguez 2017).

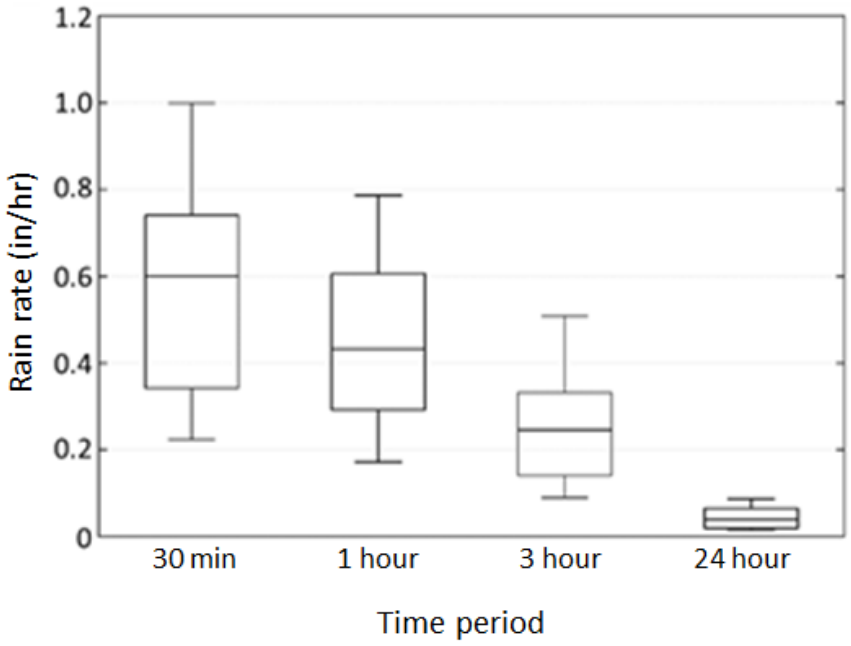

Figure 2.10. Boxplot for NYC-averaged max rainfall rates over 30-min, 1hr, 3 hr, 6 hr, and 24-hr for the 86 days of known flooding (2001-2015). Staten Island is excluded due to the blocked rain band (Figure 2.9). Whiskers represent the 10th and 90th percentiles, the box represents the 25th and 75th percentiles, and the line represents the median. Image from (Smith and Rodriguez 2017).

This article is protected by copyright. All rights reserved.

2.4.1.4 Heavy downpour projections

Predicting and understanding heavy downpours in New York City is difficult, and the science is not yet available to accurately project future heavy rainfall at one- to six-hour timescales. Short-duration heavy downpours are likely more sensitive to atmospheric conditions than longer-duration extreme rainfall, and results from longer-duration studies are not directly applicable to shorter-duration rainfall (Westra et al. 2014). Additionally, heavy downpours can vary spatially across the city, and therefore rainfall results from Central Park may not be applicable across all five boroughs. Finally, when using rainfall projections for design purposes such as in the New York City Design Guidelines, it is important to recognize that smaller areas can experience higher rainfall rates than larger areas. This is often solved for using Area Reduction Factors, which scale rainfall intensity by the areal extent of coverage (e.g. Wright et al. 2013).

Urban impacts. Heavy downpours in New York City and other cities are affected by several physical processes including urban modification of rainfall and interactions with the land-sea boundary. Patterns of urban modification of rainfall have been found in Chicago (Changnon 1968), Cleveland (Huff and Changnon 1973), St. Louis (Changnon 1979), San Antonio and Dallas (Shepherd et al. 2002), Houston (Burian and Shepherd 2005), Indianapolis (Niyogi et al. 2011), Atlanta (Wright et al. 2012, McLeod et al. 2017), Baltimore (Smith et al. 2012), and Charlotte (Wright et al. 2013).

Urban areas can change rainfall patterns through urban heat island effects, urban-induced roughness (i.e., buildings interrupting air flow), and aerosols caused by pollution (Shepherd 2005; Shepherd 2013). These effects influence the path and development of thunderstorms, resulting in different rainfall patterns depending on the atmospheric setting. Generally, a weak urban heat island increases rainfall over city centers, while strong urban heat islands increase rainfall around the urban fringe, particularly downwind of urban areas (Bornstein and LeRoy 1990; Shepherd 2013). Short-duration heavy rainfall that produces flooding in urban areas is typically driven by warm-season thunderstorms with the most extreme rain rates occurring in the evening (Ntelekos et al. 2007). These storms are also the most influenced by urbanization (Smith et al. 2013).

A handful of studies have attempted to understand the spatial patterns of observed extreme rainfall in New York City as it is impacted by urbanization. Bornstein and LeRoy (1990) investigated the impacts of the city on paths of thunderstorms. They found that the urban heat island can cause convection, or lifting of air, while the city roughness (buildings and structures) can induce divergence, or the separation of air; together these result in rainfall minima within the city and rainfall maxima surrounding and downwind of the city, especially on days with a strong urban heat island (Bornstein and LeRoy 1990).

Author Manuscript

This article is protected by copyright. All rights reserved.

Yeung used high-resolution radar rainfall fields from the Fort Dix, NJ radar and Weather Research and Forecasting modeled storm events to investigate the role of urban areas on convective storm tracks in the greater New York City region. The results showed an increased number of days exceeding 1 inch of rainfall over New York City (on average, 9 days per summer season, Yeung et al. 2011). Recently 1-hr, 4-km^2, multi-sensor Stage IV rainfall data (Lin and Mitchell 2005) were used to classify rainfall in New York City down to 1-hour events (Hamidi et al., 2017). The results showed that rainfall extremes have substantially higher rainfall rates at a 1-hour scale in the summer, and that summer extreme rainfall is more spatially concentrated and associated with localized frontal systems than is winter extreme rainfall. Furthermore, Queens is most likely, and Staten Island is least likely, to experience high intensity large areal extent 1-hr summertime precipitation extremes (Hamidi et al., 2017).

Land-sea boundary effects. The land-sea boundary also plays an important role in storm development and spatial patterns of extreme rainfall. The sea-breeze can cause air to converge at low levels, thus creating uplift for thunderstorms (Weckwerth 2000) and producing strong convection (Wilson and Megenhardt 1997). In regions with both urbanization and land-sea boundaries to the east, the land-sea boundary tends to increase convergence, provide a source of moisture for thunderstorms, and increase rainfall intensity (Ryu et al. 2016). It is difficult, however, to disentangle the effects of sea breezes and the urban influence, as urbanization can affect the location of sea-breeze fronts (Carter et al. 2012). Furthermore, New York City's location with its multiple water bodies creates an array of different sea-breeze fronts across the city (Colle et al. 2003; Novak and Colle 2006).

2.4.1.5 Effects of climate change on heavy downpours

Climate change is likely to influence the complex dynamics of urban and sea-breeze-modified heavy downpours. Heavy downpours are closely tied to the amount of available moisture in the air, which is in turn influenced by air temperature as discussed in the previous section of the chapter. As the climate warms, the Clausius-Clapeyron relationship indicates that a warmer atmosphere can have higher ratios of water vapor to air at saturation; this is likely to increase rates of heavy downpours with climate change (Trenberth et al., 2003). However, increases of rainfall intensity with temperature have been observed at much higher ratios than predicted by the Clausius-Clapeyron equation, especially for sub-daily extreme rainfall (Westra et al. 2014). It has also been projected that there will be more convective storms over the Northeast United States during the later 21st century (Li and Colle, 2016), which will additionally increase heavy downpours and flooding.

Interactions between these complex mechanisms are difficult to predict, but some paths forward have been proposed (Arnbjerg-Nielsen et al. 2013). These include a determination of the storm types that drive extreme rainfall in New York City (Figures 2.9

This article is protected by copyright. All rights reserved.

Author Manuscript

and 2.10). This will help to clarify a path forward and should be considered in future work of the NPCC.

Author Manuscript

2.4.2 Urban flooding

Increases in extreme rainfall are expected to increase urban flooding because an increase in water volume should increase flood peaks (Schrieder et al. 2000; Ashley et al. 2005; Melillo et al. 2014). At national and regional scales, however, the ability to detect this trend is difficult. Several studies have examined streamflow records for a connection between high-flow events and climate change at national and regional scales. While some studies have found significant trends in high-flow streamflow (Groisman et al., 2001a; Groisman et al., 2001b; Juckem et al., 2008; Sagarika et al., 2014) others have not (Douglas et al. 2000; McCabe and Wolock, 2002; Small et al, 2006; Villarini et al., 2009; Hirsch and Ryberg, 2011).

These studies typically analyze watersheds that are undisturbed, but a few regional studies have attempted to discern changes in the urban flood record with climate change (Yang et al., 2013 in Milwaukee; Rouge and Cai, 2014 in Chicago). Yang notes that for changes in flood response it is difficult to disentangle signals of "large-scale climate change, regional climate change induced by urbanization, and contrasting runoff generation mechanisms associated with land surface properties."

Urban flooding was not covered in NPCC2. Here, NPCC3 establishes current baselines and past trends in urban flooding for New York City and the surrounding area. These can be used in the next generation of projections for urban flooding that will be derived from quantitative projections of heavy downpours to be developed by NPCC4.

2.4.2.1 Urban flooding past trends and baselines

No dataset exists within New York City to establish past trends in urban flooding. In order to investigate trends, streamflow data for flash flooding in small watersheds near New York City was used as a proxy. Annual peak streamflows in several small (less than 15 km^2) watersheds in the U.S. Census-designated New York City urban region were analyzed for change points and statistically significant trends, similarly to the heavy downpour rainfall data.

Trends in urban flooding are difficult to establish via this flash flooding proxy (for full results see Appendix 2.E). One New York City-region stream record, for the Mahwah River near Suffern, NY, has a statistically significant change point in 1967, which is similar to the change point in rainfall extremes (see Section 2.4.1.3). A different stream, Jumping Brook near Neptune City, NJ, has a statistically significant negative trend in annual peaks. Changes in annual peaks vary across the 14 streams with both increasing and decreasing change points and trends. These changes are likely to be less representative of climate changes

This article is protected by copyright. All rights reserved.

(which would show more consistent changes across the streams) and are more representative of a direct human impact on flash flooding. Nearly all the streams are highly managed through regulations, upstream diversions, and channel modifications. These urbanization effects, including the effects of impervious surfaces (Leopold 1968), are likely to have larger impacts on the frequency and intensity of flash floods than does climate change (e.g. Yang et al., 2013 in Milwaukee; Rouge and Cai, 2014 in Chicago).

The combination of urbanization and climate change requires flooding and stormwater management to be assessed in a non-stationary framework - that is a framework in which historic flood and runoff occurrence is not strictly relied upon to predict the probability of future flooding events (Milly et al. 2008). This appears to be particularly evident with compound flooding (flooding caused by the combination of heavy downpours and storm surge) occurrence. Research has shown the number of compound flooding events in New York City to be increasing as weather patterns shift to cause more storm surge and larger precipitation amounts (Wahl et al. 2015).

Urban flooding baselines and variation across the city were analyzed using 311 flood report data (https://data.cityofnewyork.us/Social-Services/311-Service-Requests-from-2010-to-Present/erm2-nwe9). Typically, urban flooding is detected as a quick rise in stream depth or flow over a certain threshold (as used in Appendix Table 2.E.2). However, within the limits of New York City, there are no small stream channels to use for flood analyses. A major source of flood data is the 311 database, which records citizen phone calls to report street or highway flooding. Unfortunately, these 311 flood calls are biased due to two major issues. First population density differences across the city make floods much more likely to be seen and reported in dense areas of the city. Second different communities may report flooding at different rates due to perceptions of the likelihood of a response to their reports. These differences in reporting can also be observed in other types of 311 calls; for example, noise complaints, broken street lights, and other reports are also geographically biased. This underlying bias of all types of 311 reports was used to correct the bias in flooding 311 reports. The number of 311 flood calls within a 1 km^2 area around a point was divided by the number of all 311 calls within the same area (Fig. 2.11). This allows for a distinction of how often floods are reported as compared to other 311 issues Additionally, the New York City 2014 Hazard Mitigation Plan with its annual updates and flood reports from the National Climactic Data Center (NCDC, https://www.ncdc.noaa.gov/stormevents/) were used to define days of known flooding. These reports are generated by experts (National Weather Service staff and emergency managers), which can make them more accurate, but standards in reporting have changed over time and events reporting has increased in more recent years.

Baseline data based on 311 calls for urban flooding indicate substantial spatial variation across New York City from 2004 to 2015 (Fig. 2.10). Flooding appears to occur most often in areas near the coast and areas without combined sewers: Staten Island,

This article is protected by copyright. All rights reserved.

Jamaica Bay, and eastern Queens. The flooding pattern has been analysed in comparison to rainfall and other potential factors, including elevation, impervious surfaces, and population density, to determine the drivers of flooding in New York City (Smith and Rodriguez 2017). Results indicate that high groundwater tables influence flooding along the coast, while intense one-hour to one-day rainfalls cause flooding farther inland. Flooding in Staten Island is primarily caused by wintertime extratropical cyclones (Smith and Rodriguez 2017). Results from the 311 data indicate that differences in flooding across the city are likely related to rainfall patterns, proximity to the coast, impervious coverage, and differing sewer coverage. The New York City 2014 Hazard Mitigation Plan additionally includes irregular topography, soil infiltration rate, and soil storage capacity as factors that influence flooding location. Figure 2.11 indicates the similar patterns between flood occurrence and sewer type, including: combined sewers, which collect both sewage and stormwater into one system; separate sewers, which have separate systems for sewage and stormwater; parks, which do not require sewers; and other, which includes any other means of stormwater conveyance, including direct drainage into local waterways.

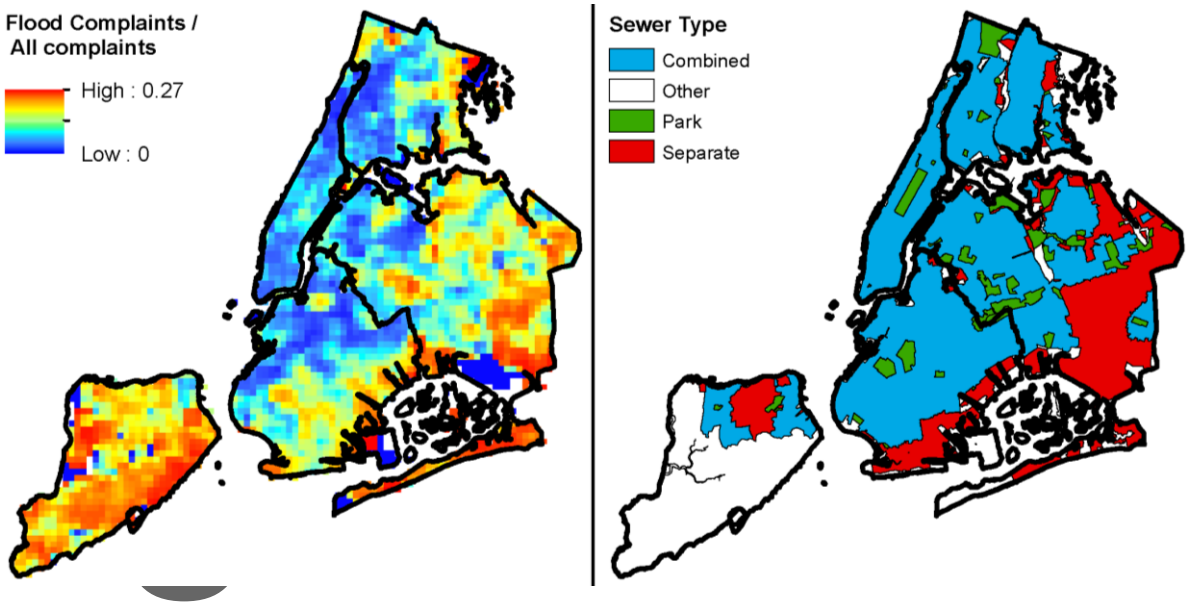

Figure 2.11. Flood observations through 311 for the period 2004–2015. Left panel: Flood observations through 311, normalized by all 311 observations. Units are in flood observations per any observation in 1 km2; Right panel: New York City sewer type. From Smith and Rodriguez (2017).

2.4.3. Future Research on Heavy Downpours and Urban Flooding

Improved projections of future heavy downpours and urban flooding in New York City will require substantially more research. Potential areas of future research include:

Heavy Downpours

This article is protected by copyright. All rights reserved.

- *Analysis of natural climate variability*. A more complete characterization of present-day variability in storms and flooding. Because the New York City region experiences such large shifts in temperatures due to the annual cycle as well as large year-to-year variability per season, it is often difficult to determine the strength of the signal of climate change to the noise of natural climate variability. Quantifying this relationship for different precipitation metrics would help decision-makers prioritize hazard-specific responses to the projected changes.

- *Precipitation Downscaling.* Results from global climate models can be dynamically downscaled, in which the outputs from the GCMs are used to force higher-resolution regional climate models (RCMs) centered around the area of interest. The RCMs should include urban features related to the New York Metropolitan Region such as its large proportion of impervious surface, tall buildings, and location near the sea. The proposed future work for extreme heat events could be used as basis for heavy downpours trends.

- Calculate trends in instances of heavy snowfall events over time in the New York metropolitan region.

-

Urban Flooding

- *Urban flood modeling.* While projecting future heavy downpours is a task that requires substantially more research, modeling urban flooding in New York City may be developed in the near future. Several open-source academic models exist or are in development (e.g., Downer and Ogden 2004, Goodrich et al. 2010, Sander et al. 2008), and commercial urban flood models (MIKE SHE, InfoWorks ICM) are available as well. Utilization of such models will allow for understanding more clearly the relationships between rainfall intensity, duration, and frequency and their effects on urban flooding in the region. These models could be used to assess current flood risks and future risks as heavy downpour projections become available.[5]

- *Increased urban flood observations.* It is difficult to determine urban flood risk in New York City and to validate urban flood models due to lack of data. Urban flooding is typically measured by depth of streamflow in small catchment streams, but this is difficult in New York City because its surface streams have been buried. Recent advances in environmental sensing using micro-controllers may indicate a path forward for urban flood data collection. In recent years, there have also been

[5] See the following website for information about the Town & Gown: Citywide Stormwater Resiliency study: https://www1.nyc.gov/assets/ddc/downloads/town-and-gown/active-rfps/Citywide Stormwater Resiliency Study T+G RFP.pdf

This article is protected by copyright. All rights reserved.

Author Manuscript

substantial efforts to identify flood risk outside the typical streamflow methods through citizen science reporting (Cheung et al. 2016; Poser and Dransch 2010).

Author Manuscript

2.5. Droughts

NPCC2 reported the potential future changes in droughts for the City using the 12-month average Palmer Drought Severity Index. It was indicated that the frequency of drought will approximately double by the 2050s and will get five times greater by the 2080s. This NPCC3 report focuses on drought indices developed for the City's major reservoir system using paleoclimate data. The drought of record in the New York Metropolitan Region is the one that occurred in the early to mid-1960s (Namias 1966). It stands as a warning of the potential vulnerability of New York City to severe water shortages. Many of the operating rules governing water management for the region depend largely on performance testing using the 1960s drought as the standard (Kolesar and Serio 2011, Devineni et al. 2013, Ravindranath et al. 2016). Since reliable observed streamflow data in the region often dates back only to the 1950s, this section addresses questions as to the long-term drought risk including the characterization of drought duration, severity and return period through paleoclimate data analyses.

Hydrologic reconstructions of streamflow from tree rings spanning the past several centuries can provide a more complete picture of the range of variability at decadal or longer time scales. Other paleoclimate studies using pollen assemblages suggest drought conditions from ~800 to 1300 AD as well (Pederson *et al.*, 2005). These paleoclimate studies can place the short instrumental record into a more long-term perspective. Previous works (Devineni et al. 2013, Woodhouse et al. 2006, Nowak et al. 2012; Stockton and Jacoby, 1976) have demonstrated the utility of paleo streamflow reconstructions in providing a more objective evaluation of operating rules for reservoir systems. Consequently, for NPCC3, we developed reconstructions of the Pepacton, Cannonsville, and Neversink (PCN) reservoirs'

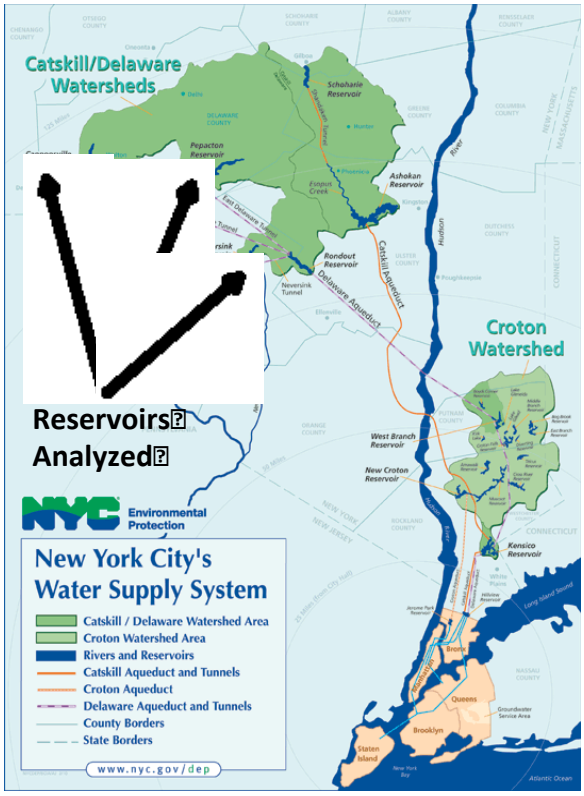

Figure 2.12. New York City's Water supply system. The Delaware watersheds Cannonsville, Pepacton and Neversink reservoirs are analyzed. *Source: NYCDEP.*

This article is protected by copyright. All rights reserved.

inflows (Figure 2.12) using tree-ring chronologies in the upper Delaware River basin[6]. We used these extended reservoir inflow records to develop long-term drought profiles on duration, severity and return periods under different demands thresholds. Table 2.8 provides key definitions for terms used to discuss drought throughout this section.

Table 2.8. NPCC3 drought definitions.

Term	Definition
Reservoir Inflow	Streamflow (amount of water) coming into the reservoirs.
Reconstructions	An estimate of streamflow for past period using trees proven to be good estimators of observed streamflow during the period of gauged record. This is typically developed using statistical models that capture the relationship between tree growth index and the observed streamflow record during the overlapping period. This statistical model is applied to the prior period.
Cumulative Deficit	The accumulated water deficit over an n-year period. The deficit for each year is defined as the difference between water demand (reservoir releases) and the water supply (reservoir inflows).

2.5.1. Methods of Analysis

This section briefly presents the methodology employed for reconstructing the reservoir inflow and for deriving the drought indicators.

2.5.1.1 Reservoir inflow reconstructions

We developed the Pepacton, Cannonsville, and Neversink reservoirs' inflow reconstructions using a statistical regression model. Instrumental data (i.e., inflows for the three reservoirs during the observation period since 1928) are provided by the New York City Department of Environmental Protection. Tree ring-width measurements that represent paleoclimate data for the Delaware watershed date back to 1754. These are available from the Tree Ring Laboratory at the Lamont-Doherty Earth Observatory (LDEO) in New York. Given data from the three reservoirs and eight local tree-ring chronologies as predictor variables, the statistical model provides regression equations for each reservoir that are used to

[6] While this NPCC report recommends using the Delaware River Basin as a drought proxy for the New York Metropolitan Region, the City measures and monitors water supply availability on a whole system basis including the Delaware, Catskill and the Croton systems.

This article is protected by copyright. All rights reserved.

Author Manuscript

reconstruct the streamflow. The period over which the reconstruction was done is 1754 – 1927. The resulting outputs are simulations of annual average daily streamflow from 1754 to 2000 for the three reservoirs. Data description and technical details of the model structure are provided in Appendix 2.F. Full details of the methods can be found in Devineni et al. (2013).

2.5.1.2 Drought Indicators

Next, we constructed a drought index to characterize the regional drought with explicit consideration of water demands. See Appendix 2.F for detailed methodology. We developed the drought index on instrumental streamflow data first to gain an understanding of the observed drought risk since 1928. Then, we applied it to the reservoir inflows reconstructed from the tree-ring data.

2.5.2. Results

This section presents the results of the streamflow reconstructions and drought analysis for the instrumental period and the paleo-reconstructed period.

2.5.2.1 Combined inflows from tree-ring data and incidence of observed drought

The general trends of combined reservoir inflow from tree-ring data from 1754-2000 are shown in Figure 2.13. While the 1960s drought in the most severe in the extended record, the tree-ring analysis show that there were regimes with less severe but longer drought durations (e.g., 1830-1860, 1790-1810).

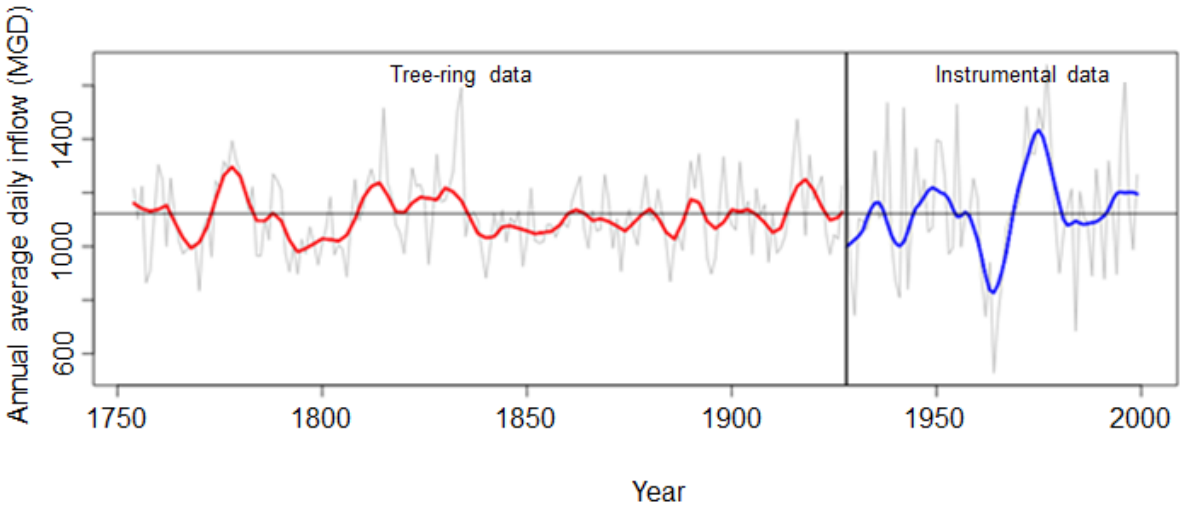

This article is protected by copyright. All rights reserved.

Author Manuscript

Figure 2.13. Reconstruction of combined annual average daily inflow from eight tree-ring chronologies in the Pepacton, Cannonsville, and Neversink reservoirs, which supply approximately 50% of the New York City water supply. Since tree growth is dependent on climate and since each tree ring represents a season of growth, tree ring measurements provide information on hydrological indicators over a tree's lifespan that can be used to understand variations in climate.

By examining this historical record, there are at least 8 incidences of historical drought lasting 5 consecutive years or longer occurring in the region since 1750 (Table 2.9). Six of these occurred in the paleo record period, and two were observed in the instrumental period. This indicates there is a potential for persistent drought in the New York Metropolitan Region in the future.

Table 2.9. Incidence of historical drought of at least 5-consecutive years in the New York Metropolitan Region in the paleo record (1754-1927) and the instrumental record (1928-1999).

Paleo record	
Drought duration	**Years**
10 years	1764-1773
11 years	1791-1801
5 years	1803-1807
9 years	1852-1860
6 years	1883-1888
5 years	1909-1913
Instrumental Record	
Drought duration	**Years**
5 years	1929-1933
7 years	1961-1967

Further discussion on the incidence of observed drought based upon annual average daily inflows and cumulative reservoir deficit can be found in Appendix 2.F.

Author manuscript

This article is protected by copyright. All rights reserved.

2.5.3. Summary and Future Work

Long-term drought risk for the New York City water supply system is developed based on the tree-ring based reconstructions for PCN reservoir inflows. The streamflow reconstructions reveal droughts with a longer duration than the duration of the major drought seen in the instrumental period (1960s drought). If the variability of streamflow as seen from the long paleoclimate tree-ring record (246 years) were to continue into the future, increases in regional demand could affect the duration of droughts. This is important from a drought risk and planning perspective.

Hydrologic reconstructions provide a more complete picture of how streamflows have varied in the New York Metropolitan Region water supply area. However, longer-term water planning decisions should also be informed by climate scenarios, such as the New York City Panel on Climate Change (Moody and Brown, 2012, Steinschneider et al. 2012). Given current understanding of seasonal to inter-annual climate variability, and of climate change, NPCC4 could develop an approach for regularly updating the drought estimates using climate observations and models tuned to prediction at different time scales. Consequently, future work should involve drought risk characterization and modeling that embraces paleo-reconstructions, climate model hindcasts and near-term projections in a rigorous way to understand climate risk and formulate management and adaptation strategies at decision relevant scales.

2.6. Conclusions and recommendations

NPCC3 confirms the use of NPCC2 projections as those of record for decision-making in the City of New York. It analyzed how recent climate trends compare to the projections for the region. Further, it has begun to develop and test new methods for observations and projections to be used in resilience planning for the region. Using expanded observations, bias correction, and regional climate models, these methods can provide quantitative analyses for heat extremes, heavy downpours, and droughts. They are available for developing the next full set of NPCC projections, which will take place after the completion of the next Intergovernmental Panel on Climate Change (IPCC) cycle, due in 2022.

Based on these and other methods, the next generation of global and regional climate model outputs will be used in upcoming NPCC assessments to create a new unified set of projections for decision-making in the New York Metropolitan Region. The methods tested by NPCC3 utilizing global and regional climate model ensembles and scenarios will enable the updated identification of climate change ‘hotspots’ of vulnerability at finer spatial scales within the City and across the region.

Projected increases in the frequencies and intensities of extreme events pose particular challenges to New York City. The six climate extremes considered in NPCC3 are

This article is protected by copyright. All rights reserved.

Author Manuscript

extreme heat and humidity, heavy downpours, droughts, sea level rise and coastal flooding, extreme winds, and cold snaps.

Author Manuscript

Key Findings

Observations and Projections

- Observed temperature trends between 2010 and 2017 fell largely within the NPCC2 projected range of heavy rainfall events for the 2020s time period encompassing the years of 2010-2039 (Fig. 2.1.a).
- Observations of increasing heavy rainfall between 2011 and 2017 fell largely within the NPCC2 projected range of extreme maximum and minimum events for the 2020s time period encompassing the years of 2010-2039 (Fig. 2.1.b).
- NPCC3 confirms the use of the NPCC2 2015 projections for decision-making by the City and region.

Extreme Heat

- Decadal trends in annual daily average maximum summer temperatures in June, July, and August varied across the City (Fig. ES.5). Central Park has experienced an increasing trend of 0.2°F per decade from 1900 to 2013. Since 1970, JFK average annual daily maximum summer temperatures have been rising at a rate of 0.5°F per decade, and 0.7°F per decade at La Guardia.
- New projection methods for extreme heat events were developed and tested for the New York Metropolitan Region. They test bias correction, a method that adjusts the mean and variance of GCM results to match a representative set of observations from the region and high-resolution regional climate modeling (Fig. 2.3).

Heavy Downpours

- NPCC3 confirms the use of NPCC2 heavy rainfall projections as those of record for City policy and planning.
- Observations from 2010 to 2017 – the period for which both observed data and NPCC2 projections are available to compare – have been largely consistent with projected range of changes in average annual and daily extreme rainfall
- NPCC2 included a qualitative projection that downpours are “very likely” to increase by the 2080s. Since NPCC2, there have been a few new studies using global climate model projections of precipitation extremes in the Northeast United States. The results from these studies are consistent with the NPCC2 Report in that they project an increase in precipitation, both in terms of the mean and extremes for the region (Ning et al., 2015). These precipitation changes are expected to occur in both the

This article is protected by copyright. All rights reserved.

winter and summer seasons (Fan et al. 2014). However, the uncertainty in these precipitation projections is larger than the uncertainty in the modeled temperature projections.

- In examining trends in sub-daily heavy rainfall events, a change point can be detected at the Central Park rain gauge in mid-1960s at 3-hr time scale for annual maximum rainfall, and the only significant trend found was for 3-hr annual maximum rainfall depth at JFK rain gauge
- Extratropical cyclones cause the largest number of extreme 24-hour precipitation events in every month out of the year.
- Rainfall that drives urban and flash flooding in the Northeast is typically temporally and spatially concentrated and is most often caused by thunderstorms.
- Days of known flooding vary spatially across New York City in rainfall depth between 0.9 to 1.25 inches. Rainfall on flooding days is at a maximum (1.25 in) over the geographic center of the city (North Brooklyn and Southeast Queens), while some areas of high rainfall extend downwind of the city to the northeast.
- Urban flooding appears to occur most often in areas near the coast and areas without combined sewers: Staten Island, Jamaica Bay, and eastern Queens. Results from the 311 data indicate that differences in flooding across the city are likely related to rainfall patterns, proximity to the coast, impervious coverage, and differing sewer coverage.
- The groundwork for future projections was established by refocusing the discussion from daily to sub-daily rainfall extremes. Heavy downpours are becoming more intense in the region. Abrupt increases of 3-hour rainfall, known as change points as they indicate that the median rainfall depth has changed, were found at the Central Park rain gauge in the mid-1960s and steady increases were found at JFK.
- Calculate trends in instances of heavy snowfall events over time in the New York metropolitan region.

Droughts

- While there has not been a major drought since the 1960s in the New York Metropolitan Region, analysis based on tree-rings from about the last 250 years shows that 10-year or longer droughts have occurred (Fig. 2.13). Thus, the possibility of future droughts should be considered in planning.

<u>Recommendations for Research</u>

This article is protected by copyright. All rights reserved.

Author Manuscript

- Relevant research areas include understanding the declining impacts of heat over time (presumably due to increased prevalence of air conditioning), continued examination of thresholds of heat and humidity effects on human health, and strategies to design projections and interventions that will be most effective in New York City's hotter climate.
- Future NPCC research can improve the utility of quantitative heat-wave projections by working with the New York City Department of Health and Mental Hygiene and the National Weather Service. Together these groups can investigate how best to evaluate need for future revisions of heat advisory criteria that consider changing combined effects of temperature and humidity (i.e., heat index). The cascading impacts of mitigation alternatives will need specific attention. Policies to mitigate extreme heat effects in population and neighborhoods at most risks are likely to lead to increases in peak and mean energy demands. Understanding these implications in the critical infrastructure should be part of mitigating policies.
- Research is needed to determine benchmarks for sub-hourly extreme precipitation and associated flooding events using satellite data and rain gauges at Central Park, LaGuardia, JFK, and Newark. Using these benchmarks, improve sub-hourly extreme precipitation projections that consider urban meteorological effects and identify neighborhoods likely to be flooded.
- Forecast and quantify uncertainties of likely large-scale conditions that may lead to extreme drought based on further tree-ring analysis in the region.

Author Manuscript

References

Anderson, G. B., and M. L. Bell, 2010: Heat waves in the United States: Mortality risk during heat waves and effect modification by heat wave characteristics in 43 U.S. Communities. *Environ. Health Perspect.*, **119**, 210–218, doi:10.1289/ehp.1002313.

Arnbjerg-Nielsen, K., P. Willems, J. Olsson, S. Beecham, A. Pathirana, I. Bülow Gregersen, H. Madsen and V.-T.-V. Nguyen, 2013: Impacts of climate change on rainfall extremes and urban drainage systems: a review, *Water Science and Technology*, 68.1, 16-28.

Arnfield, A. J., and C. S. B. Grimmond, 1998: An urban canyon energy budget model and its application to urban storage heat flux modeling. *Energy Build.*, **27**, 61–68, doi:10.1016/S0378-7788(97)00026-1.

Ashley, R. M., Balmforth, D. J., Saul, A. J., and Blanskby, J. D., 2005. Flooding in the future–predicting climate change, risks and responses in urban areas. *Water Science and Technology*, *52*(5): 265-273.

Bornstein, R. D. and G. LeRoy, 1990: Urban barrier effects on convective and frontal thunderstorms. Preprints, Fourth Conf. on Mesoscale Processes, Boulder, CO, Amer. Meteor. Soc., 120–121.

This article is protected by copyright. All rights reserved.

Boyle J. 1986. Comparison of the synoptic conditions in midlatitudes accompanying cold surges over eastern Asia for the months of December 1974 and 1978. Part I: Monthly mean fields and individual events. *Monthly Weather Review* **114**: 903–930.

Bruyère, C. L., J. M. Done, G. J. Holland, and S. Fredrick, 2014: Bias corrections of global models for regional climate simulations of high-impact weather. *Clim. Dyn.*, **43**, 1847–1856, doi:10.1007/s00382-013-2011-6.

Bruyère, C. L., J. M. Done, G. J. Holland, and S. Fredrick, 2014: Bias corrections of global models for regional climate simulations of high-impact weather. *Clim. Dyn.*, **43**, 1847–1856, doi:10.1007/s00382-013-2011-6.

Bruyère, L., Monaghan, J., Steinhoff, F., & Yates, D. (2015). Bias-corrected CMIP5 CESM data in WRF/MPAS intermediate file format.

Burian, S. and Shepard, J. (2005). Effect of urbanization on the diurnal rainfall pattern in Houston. *Hydrological Processes*, 19(5):1089–1103.

Carter, M., J. M. Shepherd, S. Burian, and I. Jeyachandran, 2012: Integration of lidar data into a coupled mesoscaleland surface model: A theoretical assessment of sensitivity of urban– coastal mesoscale circulations to urban canopy parameters. J. Atmos. Oceanic Technol., 29, 328–346, doi:10.1175/ 2011JTECHA1524.1.

Castellano, C.M. and DeGaetano, A.T., 2017: Downscaling Extreme Precipitation from CMIP5 Simulations Using Historical Analogs, *Journal of Applied Meteorology and Climatology*, *https://doi.org/10.1175/JAMC-D-16-0250.*

Castellano C and DeGaetano A (2015) Downscaled Projections of Extreme Rainfall in New York State. Northeast Regional Climate Center, Ithaca, NY.

Changnon, S.A. 1968, The LaPorte weather anomaly – fact or fiction? *Bulletin of the American Meteorological Society*, **53**, 246-251.

Changnon, S. (1979). Rainfall changes in summer caused by St. Louis. *Science*, 205:402–404.

Chen, S.; Chen, W.; Wei, K. Recent trends in winter temperature extremes in eastern China and their relationship with the Arctic Oscillation and ENSO. Adv Atmos. Sci. **2013**, 30, 1712–1724.

Cheung W, Houston D, Schubert JE, Basolo V, Feldman D, Matthew R, Sanders BF, Karlin B, Goodrich KA, Contreras SL, Luke A. Integrating resident digital sketch maps with expert knowledge to assess spatial knowledge of flood risk: A case study of participatory mapping in Newport Beach, California. Applied Geography. 2016 Sep 30;74:56-64.

Childs, P. P., and S. Raman, 2005: Observations and Numerical Simulations of Urban Heat Island and Sea Breeze Circulations over New York City. *Pure and Applied Geophysics*, **162**, 1955–1980, doi:10.1007/s00024-005-2700-0.

Colle, B. A, J. B. Olson, and J. S. Tongue, 2003: Multiseason verifi cation of the MM5. Part I: Comparison with the Eta model over the central and eastern United States and impact of MM5 resolution. Wea. Forecasting, 18, 431–457.

Author Manuscript

This article is protected by copyright. All rights reserved.

Davis, R. E., G. R. McGregor, and K. B. Enfield, 2016: Humidity: A review and primer on atmospheric moisture and human health. *Environ. Res.*, **144**, 106–116, doi:10.1016/j.envres.2015.10.014.

Downer, C. W., & Ogden, F. L. (2004). GSSHA: Model to simulate diverse stream flow producing processes. *Journal of Hydrologic Engineering*, *9*(3), 161-174.

DeGaetano, A. T., & Castellano, C. M., 2017. Future projections of extreme precipitation intensity-duration-frequency curves for climate adaptation planning in New York State. *Climate Services*, 5:23-35.

de Vries, H., Haarsma, R.J., and Hazeleger, W. (2012). Western European cold spells in current and future climate. Geophysical Research Letters. (39), L04706, doi:10.1029/2011GL050665.

Devineni, N., U. Lall, N. Pederson, and E. Cook., "A tree ring–based reconstruction of Delaware River basin Streamflow using hierarchical Bayesian regression", J. Climate, (2013), 26, 4357– 4374.

Douglas, E. M., R. M. Vogel, and C. N. Kroll (2000), Trends in floods and low flows in the United States: Impact of spatial correlation, *Journal of Hydrology,* 240, 90–105.

DRBC, Basin Information. https://www.state.nj.us/drbc/basin/ (Accessed June 15, 2018)

Efthymiadis, D.; Goodess, C.M.; Jones, P.D. Trends in Mediterranean gridded temperature extremes and large-scale circulation influences. Nat. Hazard. Earth Syst. **2011**, 11, 2199–2214.

Etienne, E., Devineni, N., Khanbilvardi, R., & Lall, U. (2016). Development of a Demand Sensitive Drought Index and its application for agriculture over the conterminous United States. Journal of Hydrology, 534, 219-229.

Fan, F., Bradley, R.S. & Rawlins, M.A. Clim Dyn (2014) 43: 145. https://doi.org/10.1007/s00382-014-2198-1

Fischer, E. M., S. I. Seneviratne, P. L. Vidale, D. Lüthi, and C. Schär, 2007: Soil Moisture–Atmosphere Interactions during the 2003 European Summer Heat Wave. *J. Clim.*, **20**, 5081–5099, doi:10.1175/JCLI4288.1.

Gao, Y., J. S. Fu, J. B. Drake, Y. Liu, and J.-F. Lamarque, 2012: Projected changes of extreme weather events in the eastern United States based on a high resolution climate modeling system. *Environ. Res. Lett.*, **7**, 044025, doi:10.1088/1748-9326/7/4/044025.

Gedzelman, S. D., S. Austin, R. Cermak, N. Stefano, S. Partridge, S. Quesenberry, and D. A. Robinson, 2003: Mesoscale aspects of the urban heat island around New York City. *Theor. Appl. Climatol.*, **75**, 29–42, doi:10.1007/s00704-002-0724-2.

Goodrich, D. C., Unkrich, C. L., Smith, R. E., Guertin, D. P., Hernandez, M., Burns, I. S., ... & Kepner, W. G. (2010). The AGWA-KINEROS2 suite of modeling tools. In *Watershed Management 2010: Innovations in Watershed Management under Land Use and Climate Change* (pp. 1294-1305).

This article is protected by copyright. All rights reserved.

Author Manuscript

Groisman, P. Y., R. W. Knight, and T. R. Karl (2001a), Heavy precipitation and high streamflow in the contiguous United States: Trends in the 20th century, *Bulletin of the American Meteorological Society,* 82, 219–246.

Groisman, P. Y., R. W. Knight, T. R. Karl, D. R. Easterling, B. Sun, and J. H. Lawrimore (2001b), Contemporary changes of the hydrological cycle over the contiguous United States: Trends derived from in situ observations, *Journal of Hydrometeorology,* 5, 64–85.

Gutiérrez, E., J. E. González, A. Martilli, R. Bornstein, and M. Arend, 2015a: Simulations of a heat-wave event in New York City using a multilayer urban parameterization. *J. Appl. Meteorol. Climatol.*, **54**, 283–301, doi:10.1175/JAMC-D-14-0028.1.

Gutiérrez, E., A. Martilli, J. L. Santiago, and J. E. González, 2015b: A Mechanical Drag Coefficient Formulation and Urban Canopy Parameter Assimilation Technique for Complex Urban Environments. *Bound.-Layer Meteorol.*, **157**, 333–341, doi:10.1007/s10546-015-0051-7.

Gutiérrez, E., A. Martilli, P. Ramamurthy, and J. González, 2016: A modeling approach for the estimation of latent heat fluxes in urban environments: Implementation and assessment. *Int. J. Climatol.*, Under Review.

Hall, T. and J. F. Booth, 2017: SynthETC: A Statistical Model for Severe Winter Storm Hazard on Eastern North America. *Journal of Climate*, 30:14, 5329-5343.

Hamidi, A., N. Devineni, J. Booth, A. Hosten, R. Ferraro, and R. Khanbilvardi, 2017: Classifying Urban Rainfall Extremes Using Weather Radar Data: An Application to the Greater New York Area. *J. Hydrometeor.,* **18**, 611–623, doi: 10.1175/JHM-D-16-0193.1.

Hass, A., K. Ellis, L. Reyes Mason, J. Hathaway, and D. Howe, 2016: Heat and Humidity in the City: Neighborhood Heat Index Variability in a Mid-Sized City in the Southeastern United States. *Int. J. Environ. Res. Public. Health*, **13**, 117, doi:10.3390/ijerph13010117.

Hawkins, E., T. M. Osborne, C. K. Ho, and A. J. Challinor, 2013: Calibration and bias correction of climate projections for crop modelling: An idealised case study over Europe. *Agric. For. Meteorol.*, **170**, 19–31, doi:10.1016/j.agrformet.2012.04.007.

Hirsch, R.M. and K.R. Ryberg (2011), Has the magnitude of floods across the USA changed with global CO2 levels? *Hydrological Sciences Journal*, 57(1), 1-9, doi:10.1080/02626667.2011.621895.

Holland, G., J. Done, C. Bruyère, C. K. Cooper, and A. Suzuki, 2010: Model Investigations of the Effects of Climate Variability and Change on Future Gulf of Mexico Tropical Cyclone Activity. Offshore Technology Conference http://www.onepetro.org/doi/10.4043/20690-MS (Accessed May 12, 2017).

Hong, S.-Y., and J.-O. J. Lim, 2006: The WRF Single-moment 6-class Microphysics Scheme (WSM6). *Asia-Pac. J. Atmospheric Sci.*, **42**, 129–151.

Haurwitz, B., 1947: Comments on the Sea Breeze Circulation. *Journal of Meteorology*, **4**, 1–8, doi:10.1175/1520-0469(1947)

Hausfather, Z., Menne, M. J., Williams, C. N., Masters, T., Broberg, R., & Jones, D. (2013). Quantifying the effect of urbanization on US Historical Climatology Network temperature records. Journal of Geophysical Research: Atmospheres, 118(2), 481-494.

This article is protected by copyright. All rights reserved.

Author Manuscript

Horton, R., D. Bader, Y. Kushnir, C. Little, R. Blake, and C. Rosenzweig, 2015: New York City Panel on Climate Change 2015 Report Chapter 1: Climate Observations and Projections: NPCC 2015 Report Chapter 1. *Ann. N. Y. Acad. Sci.*, **1336**, 18–35, doi:10.1111/nyas.12586.

Huff, F. and Changnon, S. (1973). Precipitation modification by major urban areas. *Bulletin of the American Meteorological Society*, 54:1220–1232.

Ichinose, T., K. Shimodozono, and K. Hanaki, 1999: Impact of anthropogenic heat on urban climate in Tokyo. *Atmos. Environ.*, **33**, 3897–3909, doi:10.1016/S1352-2310(99)00132-6.

Juckem, P. F., R. J. Hunt, M. P. Anderson, and D. M. Robertson (2008), Effects of climate and land management change on streamflow in the driftless area of Wisconsin, *Journal of Hydrology,* 355, 123–130.

Kain, J. S., 2004: The Kain–Fritsch convective parameterization: an update. *J. Appl. Meteorol.*, **43**, 170–181, doi:10.1175/1520-0450(2004)043<0170:TKCPAU>2.0.CO;2.

Kendall, M. G., 1975. *Rank Correlation Methods*, Charles Griffin, London.

Kimura, F., and A. Kitoh, 2007: Downscaling by pseudo global warming method. The Final Report of the ICCAP. *Final Rep.*, 43–46.

Knowlton, K., B. Lynn, R. A. Goldberg, C. Rosenzweig, C. Hogrefe, J. K. Rosenthal, and P. L. Kinney, 2007: Projecting Heat-Related Mortality Impacts Under a Changing Climate in the New York City Region. *Am J Public Health*, **97**, 2028–2034, doi:10.2105/AJPH.2006.102947.

Kolesar, P. and J. Serio., "Breaking the Deadlock: Improving Water-Release Policies on the Delaware River through Operations Research", Interfaces, (2011), 41(1): 18-34.

Konrad CE. 1996. Relationships between the intensity of cold-air outbreaks and the evolution of synoptic and planetary-scale features over North America. *Monthly Weather Review* **124**: 1067–1083.

Kretschmer, M., D. Coumou, L. Agel, M. Barlow, E. Tziperman, and J. Cohen, 2018: More-Persistent Weak Stratospheric Polar Vortex States Linked to Cold Extremes, **99,** 49-60, doi: 10.1175/bams-d-16-0259.1.

Kwon, H.-H., and U. Lall, A copula-based nonstationary frequency analysis for the 2012-2015 drought in California, Water Resources Research, doi:10.1002/2016WR018959 (2016).

Leopold, L. B. (1968). *Hydrology for urban land planning--A guidebook on the hydrologic effects of urban land use* (No. 554, pp. 1-18). US Geological Survey.

Li, H., and B. A. Colle (2016). Future changes in warm season convective storm days over the Northeastern United States using CMIP5 predictions. In press to *J. Climate*.

Li, D., and E. Bou-Zeid, 2013: Synergistic interactions between urban heat islands and heat waves: The impact in cities is larger than the sum of its parts. *J. Appl. Meteorol. Climatol.*, **52**, 2051–2064, doi:10.1175/JAMC-D-13-02.1.

Lin, Y., & Mitchell, K. E., 2005. The NCEP stage II/IV hourly precipitation analyses: Development and applications. In *19th Conf. Hydrology, American Meteorological Society, San Diego, CA, USA*.

This article is protected by copyright. All rights reserved.

Author Manuscript

Loucks, D. P., J. R. Stedinger, and D. A. Haith, Water Resource Systems Analysis, Prentice-Hall, Englewood Cliffs, N. J (1981).

Lorenz, R., E. B. Jaeger, and S. I. Seneviratne, 2010: Persistence of heat waves and its link to soil moisture memory. *Geophys. Res. Lett.*, **37**, n/a-n/a, doi:10.1029/2010GL042764.

Luber, G., and M. McGeehin, 2008: Climate Change and Extreme Heat Events. *Am. J. Prev. Med.*, **35**, 429–435, doi:10.1016/j.amepre.2008.08.021.

Lyons, B. A., A. Hasell, and N. J. Stroud, 2018: Enduring Extremes? Polar Vortex, Drought, and Climate Change Beliefs. *Environmental Communication*, **12,** 876-894, doi: 10.1080/17524032.2018.1520735.

Mann, H. B., 1945. Non-parametric tests against trend. *Econometrica*, 13: 245 – 259.

Martilli, A., A. Clappier, and M. W. Rotach, 2002: An urban surface exchange parameterisation for mesoscale models. *Bound.-Layer Meteorol.*, **104**, 261–304.

McCabe, G. J., and D. M. Wolock (2002), A step increase in streamflow in the conterminous United States, *Geophysical Research Letters,* 29*(*24*), 2185,* doi:10.1029/2002GL015999.

McLeod, J., Shepherd, M., and Konrad, C. E., 2017. Spatio-temporal rainfall patterns around Atlanta, Georgia and possible relationships to urban land cover. *Urban Climate*.

Mearns, L. O., W. J. Gutowski, R. Jones, L.-Y. Leung, S. McGinnis, A. M. B. Nunes, and Y. Qian: A regional climate change assessment program for North America.*EOS*, Vol. 90, No. 36, 8 September 2009, pp. 311-312.

Meehl, G. A., and C. Tebaldi, 2004: More intense, more frequent, and longer lasting heat waves in the 21st century. *Science*, **305**, 994–997, doi:10.1126/science.1098704.

Melillo, Jerry M., Terese (T.C.) Richmond, and Gary W. Yohe, Eds., 2014. Climate Change Impacts in the United States: The Third National Climate Assessment. U.S. Global Change Research Program, 841.

Milly, P.C., Betancourt, J., Falkenmark, M., Hirsch, R.M., Kundzewicz, Z.W., Lettenmaier, D.P. and Stouffer, R.J., 2008. Stationarity is dead: Whither water management? *Science*, *319*(5863): 573-574.

Moody, P., & Brown, C. (2012). Modeling stakeholder-defined climate risk on the Upper Great Lakes. Water Resources Research, 48(10).

Morini, E., A. Touchaei, B. Castellani, F. Rossi, and F. Cotana, 2016: The Impact of Albedo Increase to Mitigate the Urban Heat Island in Terni (Italy) Using the WRF Model. *Sustainability*, **8**, 999, doi:10.3390/su8100999.

Moss, R. H. and et al. (2010). The next generation of scenarios for climate change research and assessment. Nature, **463**, http://dx.doi.org/10.1038/nature08823.

Nakanishi, M., and H. Niino, 2006: An Improved Mellor–Yamada Level-3 Model: Its Numerical Stability and Application to a Regional Prediction of Advection Fog. *Bound.-Layer Meteorol.*, **119**, 397–407, doi:10.1007/s10546-005-9030-8.

Namias, J. (1966). Nature and possible causes of the northeastern United States drought during 1962–65. Mon. Wea. Rev, 94(9), 543-554.

This article is protected by copyright. All rights reserved.

Author Manuscript

Ning, L., E.E. Riddle, and R.S. Bradley, (2015): Projected Changes in Climate Extremes over the Northeastern United States. *J. Climate,* **28**, 3289–3310,https://doi.org/10.1175/JCLI-D-14-00150.1

Ning, L., and R. S. Bradley (2014), Winter precipitation variability and corresponding teleconnections over the northeastern United States, J. Geophys. Res. Atmos., 119, 7931–7945, doi:10.1002/ 2014JD021591.

Niyogi, D., Pyle, P., Lei, M., Arya, S., Kishtawal, C., Shepard, J., Chen, F., and Wolfe, B. (2011). Urban modification of thunderstorms: An observational storm climatology and model case study for the Indianapolis urban region. *Journal of Applied Meteorology and Climatology*, 50:1129–1144.

Novak, D. R., & Colle, B. A. (2006). Observations of multiple sea breeze boundaries during an unseasonably warm day in metropolitan New York City. *Bulletin of the American Meteorological Society*, *87*(2), 169-174.

Nowak, K., Hoerling, M., Rajagopalan, B., & Zagona, E. (2012). Colorado River basin hydroclimatic variability. Journal of Climate, 25(12), 4389-4403.

Ntelekos, A. A., Smith, J. A., and Krajewski, W. F. (2007). Climatological Analyses of thunderstoms and flash floods in the Baltimore Metropolitan region. *Journal of Hydrometeorology*, 8:88–101.

Offerle, B., C. S. B. Grimmond, and K. Fortuniak, 2005: Heat storage and anthropogenic heat flux in relation to the energy balance of a central European city centre. *Int. J. Climatol.*, **25**, 1405–1419, doi:10.1002/joc.1198.

Oke, T. R., 1982: The energetic basis of the urban heat island. *Q. J. R. Meteorol. Soc.*, **108**, 1–24, doi:10.1002/qj.49710845502.

Oke, T. R., B. D. Kalanda, and D. G. Steyn, 1981: Parameterization of heat storage in urban areas. *Urban Ecol.*, **5**, 45–54, doi:10.1016/0304-4009(81)90020-6.

Ortiz, L. E., J. E. Gonzalez, W. Wu, M. Schoonen, J. Tongue, and R. Bornstein, 2018: New York City Impacts on a Regional Heat Wave. *Journal of Applied Meteorology and Climatology*, **57**, 837–851, doi:10.1175/JAMC-D-17-0125.1.

Overland, J., J. A. Francis, R. Hall, E. Hanna, S.-J. Kim, and T. Vihma, 2015: The Melting Arctic and Midlatitude Weather Patterns: Are They Connected? *J. Climate*, **28,** 7917-7932, doi: 10.1175/jcli-d-14-00822.1.

Pederson, D., Peteet, D., Kurdyla, D., & Guilderson, T. (2005). Medieval Warming, Little Ice Age, and European impact on the environment during the last millennium in the lower Hudson Valley, New York, USA. *Quaternary Research, 63*(3), 238-249. doi:10.1016/j.yqres.2005.01.001

Peterson, T.C.; Zhang, X.; Brunet India, M.; Vázquez Aguirre, J.L. Changes in North American extremes derived from daily weather data. J. Geophys. Res. Atmos. **2008**, 113.

Pettitt, A. N., 1979. A non-parametric approach to the change-point problem. *Appl. Stat*., 28: 126 – 135.

This article is protected by copyright. All rights reserved.

Author Manuscript

Poser K, Dransch D. Volunteered geographic information for disaster management with application to rapid flood damage estimation. Geomatica. 2010;64(1):89-98.

Rouge, C. and X. Cai (2014), Crossing-scale hydrological impacts of urbanization and climate variability in the Greater Chicago Area, *Journal of Hydrology*, 517, 13-27, doi:10.1016/j.jhydrol.2014.05.005.

Piani, C., G. P. Weedon, M. Best, S. M. Gomes, P. Viterbo, S. Hagemann, and J. O. Haerter, 2010: Statistical bias correction of global simulated daily precipitation and temperature for the application of hydrological models. *J. Hydrol.*, **395**, 199–215, doi:10.1016/j.jhydrol.2010.10.024.

Ramamurthy, P., T. Sun, K. Rule, and E. Bou-Zeid, 2015: The joint influence of albedo and insulation on roof performance: An observational study. *Energy Build.*, **93**, 249–258, doi:10.1016/j.enbuild.2015.02.040.

Ramamurthy, P., and E. Bou-Zeid, 2016: Heatwaves and Urban Heat Islands: A Comparative Analysis of Multiple Cities Using a High-Resolution Numerical Model: Heatwaves and Urban Heat Islands. *Journal of Geophysical Research: Atmospheres*, doi:10.1002/2016JD025357. http://doi.wiley.com/10.1002/2016JD025357 (Accessed December 31, 2016).

Ramamurthy, P., J. González, L. Ortiz, M. Arend, and F. Moshary, 2017: Impact of heatwave on a megacity: an observational analysis of New York City during July 2016. *Environ. Res. Lett.*, **12**, 054011, doi:10.1088/1748-9326/aa6e59.

Ravindranath, A., Devineni, N., & Kolesar, P. (2016). An environmental perspective on the water management policies of the Upper Delaware River Basin. Water Policy, 18(6), 1399-1419.

Riahi, K., and Coauthors, 2011: RCP 8.5—A scenario of comparatively high greenhouse gas emissions. *Climatic Change*, **109**, 33, doi:10.1007/s10584-011-0149-y.

Rothfusz, L. P., 1990: *The heat index equation (or, more than you ever wanted to know about heat index)*. NWS Southern Region Headquarters, Forth Worth, TX.

Rosenthal, J. K., Kinney, P. L., & Metzger, K. B. (2014). Intra-urban vulnerability to heat-related mortality in New York City, 1997–2006. Health & place, 30, 45-60.Ryu, Y. H., Smith, J. A., Bou-Zeid, E., & Baeck, M. L. (2016). The Influence of Land Surface Heterogeneities on Heavy Convective Rainfall in the Baltimore–Washington Metropolitan Area. *Monthly Weather Review*, *144*(2), 553-573.

Sailor, D. J., 2001: Relating residential and commercial sector electricity loads to climate—evaluating state level sensitivities and vulnerabilities. *Energy*, **26**, 645–657, doi:10.1016/S0360-5442(01)00023-8.

Sagarika, S., A. Kalra, S. Ahmad (2014), Evaluating the effect of persistence on long-term trends and analyzing step changes in streamflows of the continental United States, *Journal of Hydrology,* 517*,* 36.

Salamanca, F., A. Krpo, A. Martilli, and A. Clappier, 2010: A new building energy model coupled with an urban canopy parameterization for urban climate simulations—Part I.

This article is protected by copyright. All rights reserved.

Author Manuscript

Formulation, verification, and sensitivity analysis of the model. *Theor. Appl. Climatol.*, **99**, 331–344, doi:10.1007/s00704-009-0142-9.

Santamouris, M., 2014: On the energy impact of urban heat island and global warming on buildings. *Energy Build.*, **82**, 100–113, doi:10.1016/j.enbuild.2014.07.022.

Schaeffer, R., et al., 2012: Energy sector vulnerability to climate change: A review. *Energy*, **38**, 1–12, doi:10.1016/j.energy.2011.11.056.Screen, J. A., and I. Simmonds, 2010: The central role of diminishing sea ice in recent Arctic temperature amplification. *Nature*, **464,** 1334, doi: 10.1038/nature09051 https://www.nature.com/articles/nature09051#supplementary-information.

Screen, J. A., C. Deser, and L. Sun, 2015: Reduced Risk of North American Cold Extremes due to Continued Arctic Sea Ice Loss. *Bull. Am. Meteorol. Soc.*, **96,** 1489-1503, doi: 10.1175/bams-d-14-00185.1.

Screen, J. A., T. J. Bracegirdle, and I. J. C. C. C. R. Simmonds, 2018: Polar Climate Change as Manifest in Atmospheric Circulation. *Current Climate Change Reports*, doi: 10.1007/s40641-018-0111-4.

Seneviratne, S. I., D. Lüthi, M. Litschi, and C. Schär, 2006: Land–atmosphere coupling and climate change in Europe. *Nature*, **443**, 205–209, doi:10.1038/nature05095.

Sen, P.K., 1968. Estimates of the regression coefficient based on Kendall's tau. *Journal of the American Statistical Association,* 63: 1379–1389.

Seo, B.C., Krajewski, W.F., Kruger, A., Domaszczynski, P., Smith, J.A. and Steiner, M., 2011. Radar-rainfall estimation algorithms of Hydro-NEXRAD. *Journal of Hydroinformatics*, *13*(2), pp.277-291.

Shepherd, J. M., 2013. Impacts of urbanization on precipitation and storms: Physical insights and vulnerabilities. *Climate Vulnerability, 5: 109-125*.

Shepherd, J. M., 2005. A review of the current investigations of urban-induced rainfall and recommendations for the future. *Earth Interactions*, 9.

Shepherd, J. M., Pierce, H., and Negri, A. J. (2002). Rainfall modification by major urban areas: Observations from spaceborne rain radar on the TRMM satellite. *Journal of Applied Meteorology*, 41:689–701.

Skamarock, W., Klemp, J., Dudhia, J., Gill, D., Barker, D., Wang, W., Huang, X., and Duda, M., 2008: A description of the Advanced Research WRF version 3. doi:10.5065/D68S4MVH. http://dx.doi.org/10.5065/D68S4MVH.

Small, D., S. Islam, and R. M. Vogel (2006), Trends in precipitation and streamflow in the eastern US: Paradox or perception? *Geophysical Research Letters,* 33, L03403, doi:10.1029/2005GL024995.

Smith, B., and Rodriguez, S., 2017. Spatial Analysis of High-Resolution Radar Rainfall and Citizen-Reported Flash Flood Data in Ultra-Urban New York City. *Water*, *9*(10): 736.

Smith, B. K., & Smith, J. A. (2015). The flashiest watersheds in the contiguous United States. *Journal of Hydrometeorology*, *16*(6), 2365-2381.

This article is protected by copyright. All rights reserved.

Smith, B. K., Smith, J. A., Baeck, M. L., Villarini, G., and Wright, D. B. (2013). Spectrum of storm event hydrologic response in urban watersheds. *Water Resources Research*, 49:2649–2663.

Smith, J. A., Baeck, M. L., Villarini, G., Welty, C., Miller, A. J., and Krajewski,W. F. (2012). Analysis of a long-term, high-resolution radar rainfall data set for the Baltimore metropolitan area. *Water Resources Research*, 48(W04504):1–14.

Steinschneider, S., & Brown, C. (2012). Dynamic reservoir management with real-option risk hedging as a robust adaptation to nonstationary climate. Water Resources Research, 48(5).

Stockton, C. W., and G. C. Jacoby., "Long-term surface-water supply and streamflow trends in the Upper Colorado River Basin based on treering analyses". Lake Powell Res. Proj. (1976), Bull. 18, 70 pp., Res. Appl. to Natl. Needs, Natl. Sci. Found., Arlington, Va.

Taha, H., 1997: Urban climates and heat islands: albedo, evapotranspiration, and anthropogenic heat. *Energy Build.*, **25**, 99–103, doi:10.1016/S0378-7788(96)00999-1.

——, H. Akbari, A. Rosenfeld, and J. Huang, 1988: Residential cooling loads and the urban heat island—the effects of albedo. *Build. Environ.*, **23**, 271–283, doi:10.1016/0360-1323(88)90033-9.

Tewari, M., and Coauthors, 2004: Implementation and verification of the unified NOAH land surface model in the WRF model. 20th conference on weather analysis and forecasting/16th conference on numerical weather prediction, Seattle, WA, 11–15.

Thibeault, J.M. and Seth, A. (2014). Changing climate extremes in the Northeast United States: observations and projections from CMIP5. Climatic Change 127. DOI 10.1007/s10584-014-1257-2.

Thomson, A. M., and Coauthors, 2011: RCP4.5: a pathway for stabilization of radiative forcing by 2100. *Climatic Change*, **109**, 77, doi:10.1007/s10584-011-0151-4.

Towey, K. L., J. F. Booth, A. Frei, and M. R. Sinclair, 2018. Track and Circulation Analysis of Tropical and Extratropical Cyclones that Cause Strong Precipitation and Streamflow Events in the New York City Watershed. *Journal of Hydrometeorology*.

Trenberth, K. E., A. Dai, R. M. Rasmussen, and D. B. Parsons (2003). The Changing Character of Precipitation. Bull. Amer. Meteor. Soc., 84, 1205–1217.

U. S. Census Bureau: QuickFacts New York city, New York. https://www.census.gov/quickfacts/fact/table/newyorkcitynewyork#viewtop. (Accessed June 15, 2018)

USGS, Office of the Delaware River Master, Flexible Flow Management Program (FFMP2017). https://webapps.usgs.gov/odrm/ (Accessed June 15, 2018)

Villarini, G., F. Serinaldi, J. A. Smith, and W. F. Krajewski (2009), On the stationarity of annual flood peaks in the continental United States during the 20th century, *Water Resources Research,* 45, *W08417, doi:*10.1029/2008WR007645.

Author Manuscript

This article is protected by copyright. All rights reserved.

Wahl, T., Jain, S., Bender, J., Meyers, S. D., and Luther, M. E., 2015. Increasing risk of compound flooding from storm surge and rainfall for major US cities. *Nature Climate Change*, *5*(12): 1093-1097.

Walsh, J., D. Wuebbles, K. Hayhoe, J. Kossin, K. Kunkel, G. Stephens, P. Thorne, R. Vose, M. Wehner, J. Willis, D. Anderson, S. Doney, R. Feely, P. Hennon, V. Kharin, T. Knutson, F. Landerer, T. Lenton, J. Kennedy, and R. Somerville, 2014: Ch. 2: Our Changing Climate. Climate Change Impacts in the United States: The Third National Climate Assessment, J. M. Melillo, Terese (T.C.) Richmond, and G. W. Yohe, Eds., U.S. Global Change Research Program, 19-67. doi:10.7930/J0KW5CXT.

Weckwerth, T. M., 2000: The effect of small-scale moisture variability on thunderstorm initiation. Mon. Wea. Rev., 128, 4017–4030, doi:10.1175/1520-0493(2000)129,4017: TEOSSM.2.0.CO;2.

Westra, S., Fowler, H.J., Evans, J.P., Alexander, L.V., Berg, P., Johnson, F., Kendon, E.J., Lenderink, G. and Roberts, N.M., 2014. Future changes to the intensity and frequency of short-duration extreme rainfall. *Reviews of Geophysics*, *52*(3), pp.522-555.

Wilson, J. W., and D. L. Megenhardt, 1997: Thunderstorm initiation, organization, and lifetime associated with Florida boundary layer convergence lines. Mon. Wea. Rev., 125, 1507–1525, doi:10.1175/1520-0493(1997)125,1507: TIOALA.2.0.CO;2.

Wright, D. B., Smith, J. A., Villarini, G., and Baeck, M. L. (2012). The hydroclimatology of flash flooding in Atlanta. *Water Resources R*, 48(W04524):1–14.

Wright, D. B., Smith, J. A., Villarini, G., and Baeck, M. L. (2013). Long-term high resolution radar rainfall fields for urban hydrology. *Journal of the American Water Resources Association*, 50(3):713–734.

Woodhouse, C. A., S. T. Gray, and D. M. Meko, "Updated streamflow reconstructions for the Upper Colorado River Basin", Water Resour. Res., (2006) 42, W05415, doi:10.1029/2005WR004455.

Yang, L., J.A. Smith, D.B. Wright, M.L. Baeck, G. Villarini, F. Tian, and H. Hu (2013), Urbanization and Climate Change: An Examination of Nonstationarities in Urban Flooding, *Journal of Hydrometeorology*, 14, 1791–1809, doi:http://dx.doi.org/10.1175/JHM-D-12-095.1 .

Yeung, J.K., Smith, J.A., Villarini, G., Ntelekos, A.A., Baeck, M.L. and Krajewski, W.F., 2011. Analyses of the warm season rainfall climatology of the northeastern US using regional climate model simulations and radar rainfall fields. *Advances in Water Resources*, *34*(2), pp.184-204.

Zhang, P., Y. Wu, I. R. Simpson, K. L. Smith, X. Zhang, B. De, and P. Callaghan, 2018: A stratospheric pathway linking a colder Siberia to Barents-Kara Sea, sea ice loss. *Science Advances*, **4**, doi: 10.1126/sciadv.aat6025 %J Science Advances.

Zhang, R., Chen, Z.Y., Ou, C.Q., and Zhuang, Y. (2017). Trends of heat waves and cold spells over 1951–2015 in Guangzhou, China. Atmosphere 2017, 8, 37; doi:10.3390/atmos8020037.

This article is protected by copyright. All rights reserved.

Author Manuscript

Appendix 2.A. Global Climate Models Used in NPCC3 Ensemble for Extreme Heat and Humidity

Table 2.A.1. Global Climate Models Used in NPCC3 Ensemble for Extreme Heat and Humidity

Center	Model
Commonwealth Scientific and Industrial Research Organization – Bureau of Meteorology (Australia)	ACCESS1-0 ACCESS1-3
Canadian Centre for Climate Modeling and Analysis (Canada)	CanESM2
National Center for Atmospheric Research (USA)	CCSM4
Centro Euro-Mediterraneo per i Cambiamenti Climatici (Italy)	CMCC-CM CMCC-CMS
Centre National de Recherches Météorologiques/Centre Eurorpéen de Rechercheet Formation Avencée en Calcul Scientifique (France)	CNRM-CM5
Commonwealth Scientific and Industrial Research Organization/Queensland Climate Change Centre of Excellence (Australia)	CSIRO-Mk3-6-0
NOAA Geophysical Fluid Dynamics Laboratory (USA)	GFDL-ESM2G GFDL-ESM2M
NASA Goddard Institute for Space Studies (USA)	GISS-CM3 GISS-E2-H GISS-E2-R
Met Office Hadley Centre (UK)	HadGEM2-AO HadGEM2-CC HadGEM2-ES
Institut Pierre-Simon Laplace (France)	IPSL-CM5A-LR IPSL-CM5A-MR IPSL-CM5B-LR
Japan Agency for Marine-Earth Science and Technology, Atmosphere and Ocean Research Institute/National Institute for Environmental Studies/Japan Agency for Marine-Earth Science and Technology (Japan)	MIROC-ESM MIROC-ESM-CHEM MIROC5
Max Planck Institure for Technology (Germany)	MPI-ESM-LR MPI-ESM-MR
Meteorological Research Institute (Japan)	MRI-CGCM3
Institute for Numerical Mathematics (Russia)	INM-CM4

Author Manuscript

This article is protected by copyright. All rights reserved.

Appendix 2.B. NPCC2 vs NPCC3 projected heat extremes

Table 2.B.1. Heat wave projections across 52-member ensemble (26 models, 2 projections) for New York City. Baseline refers to 1973-2002 average characteristics.

		Baseline	10th	25th	75th	90th
Heat waves per year *Average # events per year*	2020s	1.3 (2)	0 (2)	1 (3)	4 (4)	5 (4)
	2050s	1.3 (2)	2 (4)	3 (5)	5 (7)	6 (7)
	2080s	1.3 (2)	2 (5)	3 (5)	6 (9)	7 (9)
Mean heat wave duration *Average heat wave length in days*	2020s	4 (4)	3 (4)	4 (5)	6 (7)	8 (7)
	2050s	4 (4)	4 (4)	5 (5)	9 (6)	13 (6)
	2080s	4 (4)	5 (4)	6 (5)	15 (7)	28 (8)
Mean heat wave intensity *Maximum temperature during the heat wave event in °F*	2020s	95.8	92.1	93.4	97.6	99.8
	2050s	95.8	93.3	94.9	99.2	101.8
	2080s	95.8	93.4	95.4	100	102.8
Days above 90°F *Average # days per year*	2020s	11.1 (18)	6 (24)	12 (36)	26 (31)	36 (33)
	2050s	11.1 (18)	16 (32)	25 (39)	47 (52)	57 (59)
	2080s	11.1 (18)	24 (38)	35 (44)	63 76)	75 (87)
Days above 100°F *Average # days per year*	2020s	0.28 (0.4)	0 (0.7)	0 (1)	0 (2)	2 (2)
	2050s	0.28 (0.4)	0 (2)	0 (3)	4 (5)	8 (7)
	2080s	0.28 (0.4)	0 (2)	0 (4)	13 (14)	27 (20)

Author Manuscript

This article is protected by copyright. All rights reserved.

Appendix 2.C. NPCC3 Bias Correction Methods for Heat Waves.

The bias correction technique corrects for both differences in model mean and standard deviation using a linear model, or:

$$T_{BC} = \bar{O}_{REF} + \frac{\sigma_{O,REF}}{\sigma_{T,REF}}(T_{RAW}(t) - \bar{T}_{REF})$$

Here, T_{BC} refers to the bias corrected temperature record, *O* refers to the observations from the selected stations, σ is the standard deviation, and the subscripts *REF* and *RAW* refer to the reference period and the entire projection record, respectively. The mean values of the four urban stations are used as observations for the training period of 2006-2015 for each model of the ensemble. The correction is then carried on for the three 30-years periods of interest (2020; 2050; 2080). The bias corrected distributions are presented in Figure 2.C.1 for the complete ensemble of GCM daily maximum temperatures, which shows the bias-corrected distributions are much closer to the observations.

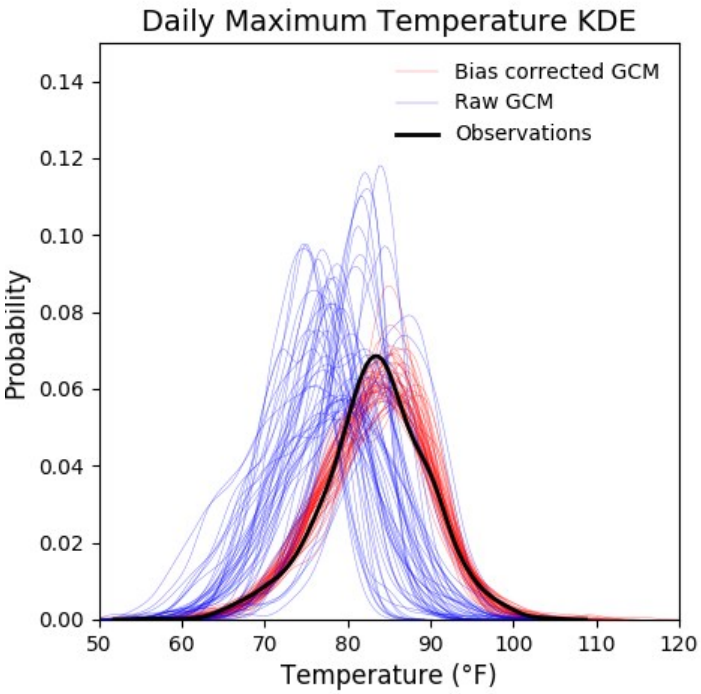

Figure 2.C.1. Sample of bias-corrected GCM distributions for maximum temperatures for the training period of 2006-2015. KDE refers to a Kernel Density Estimate, a representation of the probability of occurrence of a given value in the data set.

Appendix 2.D. Potential New Methods for NPCC4 Extreme Heat Projections

The output from global climate models (GCMs) can be dynamically downscaled, in which GCM outputs are used to drive high-resolution regional climate models (RCMs). This

This article is protected by copyright. All rights reserved.

approach has led to development of regional, or limited area models (Dickinson et al. 1989; Giorgi et al. 1993; Skamarock et al. 2008). This is a potential method for the next generation of NPCC climate change projections for New York City for use in adaptation planning and implementation. It can be a useful approach because GCMs used for quantifying future changes currently do not have adequate resolution to realistically simulate many extreme weather events, such as tropical storms, rapidly deepening nor'easters, severe convective storms, and heavy rainfall. Since these models are often run at 100-300 km grid spacing, much of the uncertainty originates from not properly resolving atmospheric dynamics near for these weather. Further, global climate model physics have large uncertainties at coarse resolution, since they do not resolve finer-scale processes such as the urban heat island and sea breezes.

Dynamical downscaling uses output from GCMs as initial and boundary conditions for high-resolution model run centered on the region of interest. In order to resolve clouds and urban-specific processes (e.g., anthropogenic heat and radiation blocking), this will require resolutions around 4-km grid spacing or less; however, most current downscaling simulations use ~20-km grid spacing. To address uncertainties in dynamically downscaled simulations, multi-simulation ensembles are employing varying boundary conditions, physics parameterizations, and grid spacing should be employed. Examples of this ensemble approach include the North American Regional Climate Change Assessment Program (NARCCAP, Mearns et al. 2009) for the contiguous US at 50 km resolution.

Another approach is using pseudo-global warming (PGW; Kimura and Kitoh 2007). In the PGW approach, the ensemble mean monthly temperature changes from the GCMs are added to the historical reanalysis data, which in turn is used for ICs/BCs for the future high-resolution regional domain runs. This approach is cheaper, since separate runs are not needed for each GCM, but this approach does not include any large-scale flow changes in the future from the GCM, since only temperature perturbations are added.

2.D.1 High Resolution Dynamical Downscaling

To test the approach in for the New York Metropolitan Region, GCM projections are downscaled using an urbanized version of the Weather Research and Forecast Model (WRF, Skamarock et al. 2008) developed and maintained by the National Center for Atmospheric Research (NCAR). Model physics are based on Gutiérrez et al. (2015a) and are summarized in Table 2.D.2. In contrast to GCMs, dynamical downscaling is performed by embedding, or nesting, models of higher spatial complexity within each other. In this case, three domains (1 parent, 2 nested) are used, with horizontal grid spacing of 9 km, 3 km, and 1 km (Figure 2.D.1). The high-resolution domain covers the New York Metropolitan Region with results presented for New York City.

Urban parameterizations require use of urban canopy parameters, such as urban land

This article is protected by copyright. All rights reserved.

Author Manuscript

use, building plant area fraction (Figure 2.D.1, left), and building heights (Figure 2.D.1, right) to represent energy and momentum exchanges between the atmosphere and built environment (Figure 2.D.1). These parameters have been derived from the Property Land Use Tax-lot Output (PLUTO) (New York City Department of City Planning 2013) made publicly available since 2013.

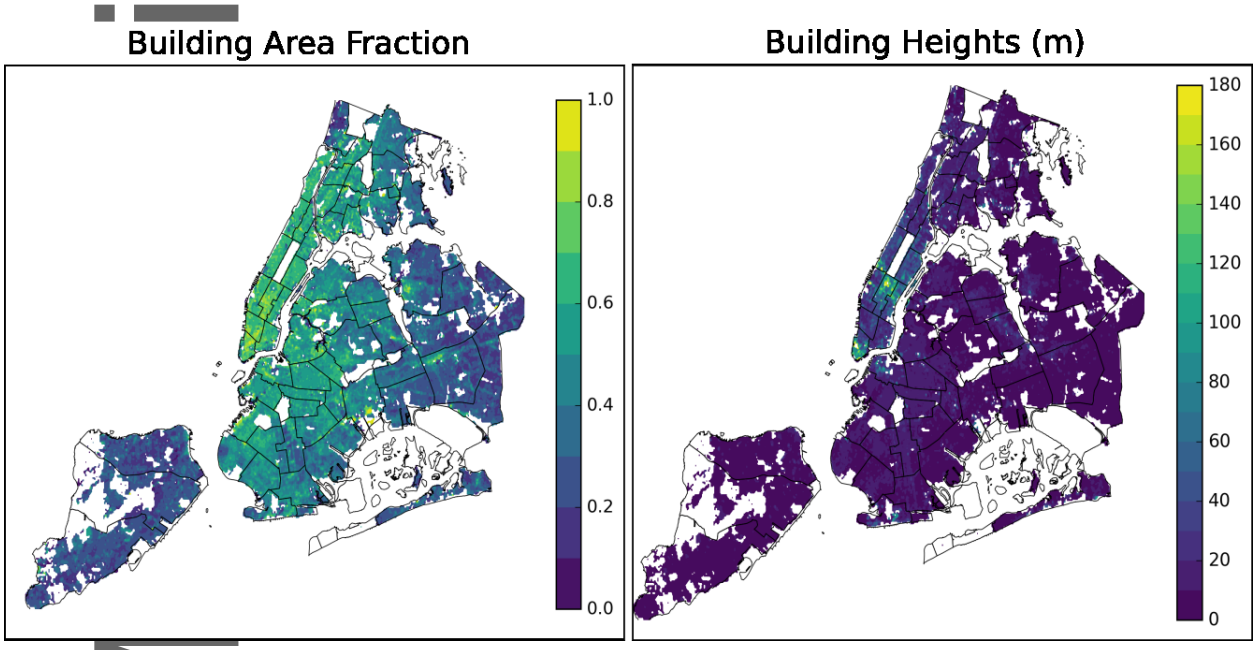

Figure 2.D.1. Urban canopy parameters for NYC derived from PLUTO. These parameters are used to calculate interactions between the atmosphere and buildings.

Table 2.D.1 Summary of approach used for regional climate model simulations.

Simulation Approach	
Regional Climate Model	Weather Research and Forecasting (WRF) model version 3.8
Initial and boundary conditions	Community Earth System Model version 1 (CESM1)
Baseline years	2006-2010
Simulation period	June 1st to August 31st
Scenarios	RCP4.5 (medium emissions) RCP8.5 (high emissions)

Table 2.D.2. Physics options used in WRF simulations.

This article is protected by copyright. All rights reserved.

Parameterization	Reference
Convection	Kain-Fritsch (Kain 2004)
Microphysics	WSM6 (Hong and Lim 2006, p. 6)
Boundary Layer	Mellow-Yamada-Janjic (Nakanishi and Niino 2006)
Land Surface	Noah land surface model (Tewari et al. 2004)
Urban Physics	BEP (Martilli et al. 2002) BEM (Salamanca et al. 2010) Cooling Tower (Gutiérrez et al. 2016) Urban Drag Coefficient (Gutiérrez et al. 2015b)

Model initial and boundary conditions are taken from a bias-corrected CESM dataset provided by NCAR (Bruyère et al. 2015), which corrects biases in the intra-annual variation for all meteorological variables using ERA-Interim Reanalysis. The bias correction technique follows the work from Holland et al. (2010) as applied by Bruyère et al. (2014). The correction method separates the GCM and Reanalysis signal into a seasonally-varying term and a perturbation term (containing the model's climate signal). The seasonal mean is the corrected using the reanalysis's historical seasonally varying mean, while keeping the model's climate perturbation. This method was found by Bruyère et al. (2014) to produce more realistic patterns of wind shear and tropical cyclone generation for the historic period. The projection ensemble is summarized in Table 2.D.1. Correcting all model variables was shown to decrease CESM1 cold temperature biases when used as input to a regional model. Finally, three time periods are selected[7]: historical (2006-2010), mid-century (2045-2049), and end of century (2095-2099).

2.D.2 RCM Results

Spatial variation of heat wave changes is shown for two time slices (2045-2049 and 2095-2099) (Figure 2.D.2) for a typical year (i.e., median values). In general, sea breeze fronts, which typically develop in the afternoon due to land-ocean air temperature differences, play a crucial role in determining projected changes by moderating high temperatures near the coast.

[7] Current computational power limits high resolution RCM simulations to relatively time slices compared to those presented at the GCM level. However, the authors feel that the added spatial granularity provide significant value.

This article is protected by copyright. All rights reserved.

Author Manuscript

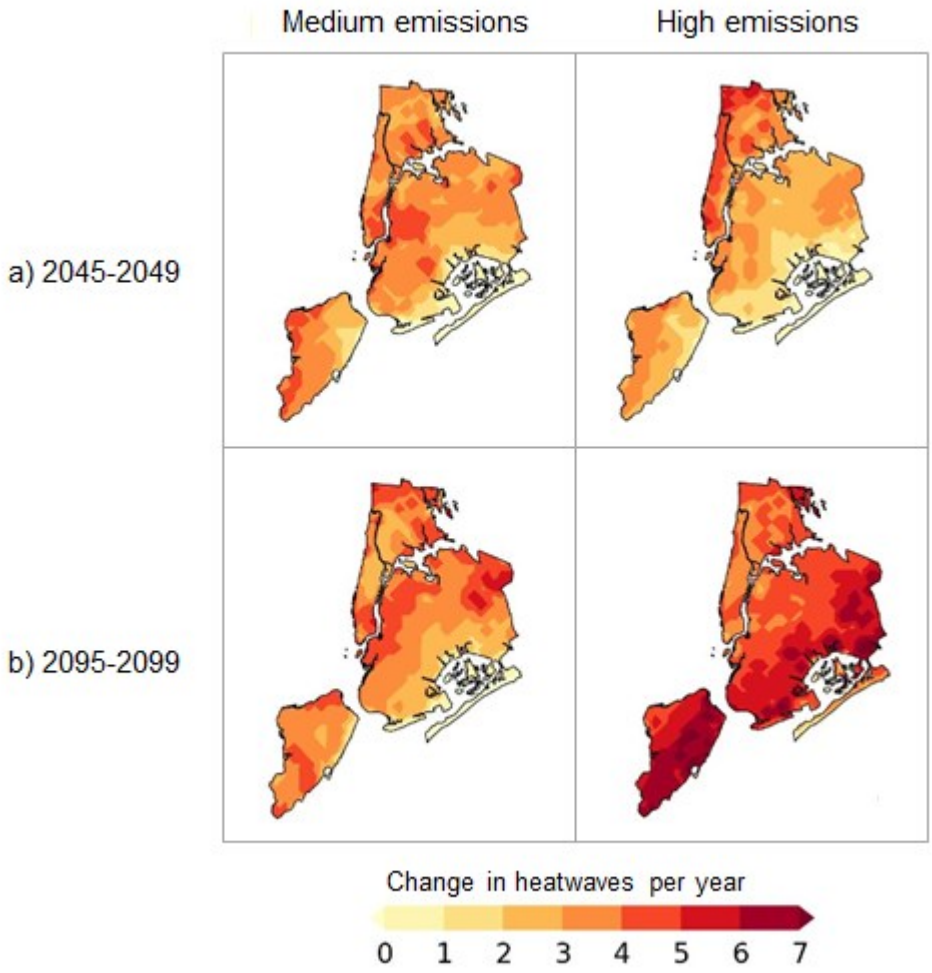

Figure 2.D.2. Median projections of event frequency for New York City.

The RCM simulations show that the number of heatwaves per year are projected to stabilize after 2045 in the medium-emissions scenario. This stabilization occurs because the land surface warms more than the ocean and this differential warming causes sea breezes to moderate the number of heatwaves that take place. This is similar to current conditions in which sea breeze circulations prevent parts of Brooklyn and Queens from experiencing as many and as severe heatwaves as parts of Manhattan and the Bronx. Projections for Manhattan and The Bronx, however, show increases in heatwaves by 2-4 events per year for both time periods.

In the high-emissions scenario (RCP8.5), the sea breeze is weakened due to increased ocean air temperatures, leading to Brooklyn and Queens experiencing higher event frequencies of between 5-7 additional events per year. This is even greater than projected heatwave increases in Manhattan and The Bronx of 4-6 events. Larger increases near the coast may also be due to historically lower temperatures due to the local sea breeze.

Author M

This article is protected by copyright. All rights reserved.

The heat index (Rothfusz 1990), combining temperature and relative humidity, is often used as a metric of how heat affects humans. Projections show that the heat index is expected to increase with time across projections, with end of century changes ranging between 6-8°F in medium-emissions scenario to 12-16°F in high-emissions scenario (Figure 2.D.3). Changes in heat index are, in general, slightly larger over Manhattan and the northern part of Brooklyn in all scenarios and time slices except in end of century high-emissions scenario, where a similar pattern as that observed in event frequency projections emerges, with heat index increasing at a faster rate towards the coast.

Author Manuscript

This article is protected by copyright. All rights reserved.

Author Manuscript

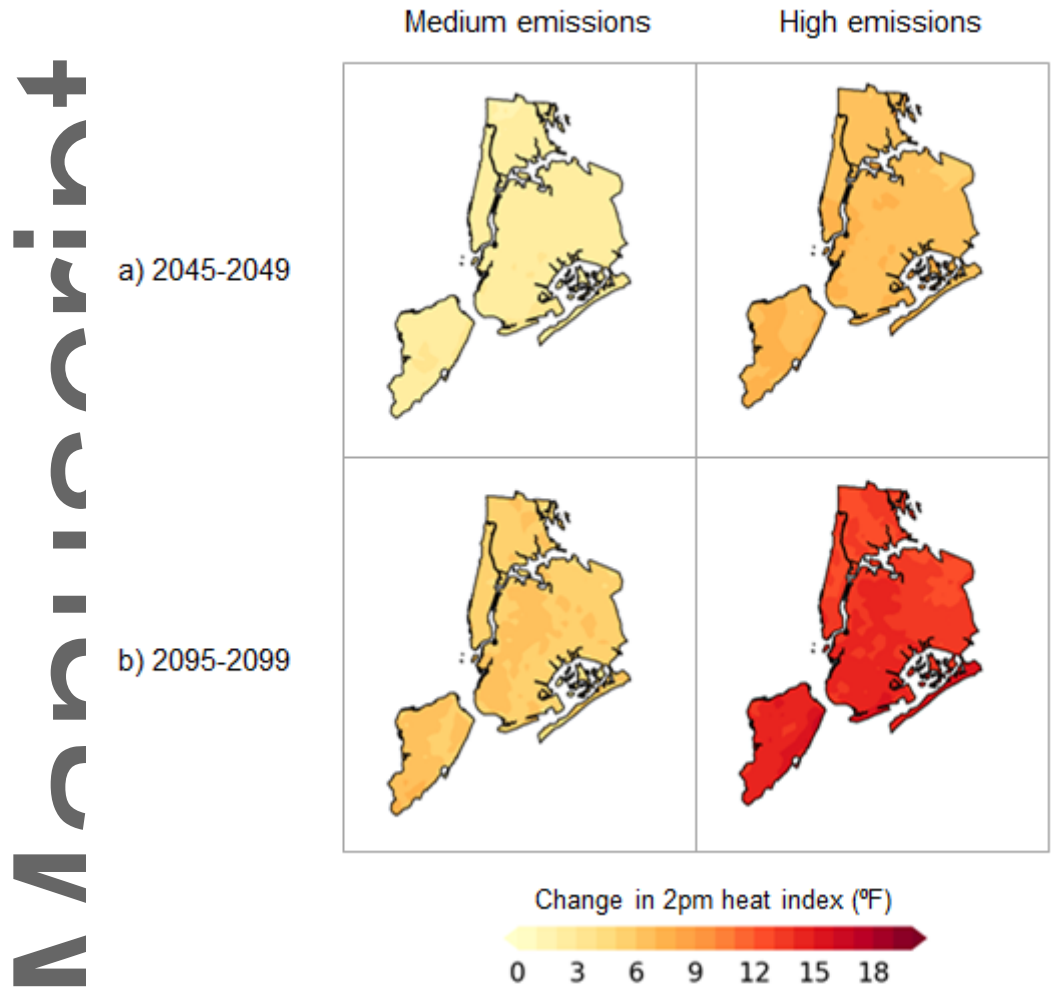

Figure 2.D.3. Median 2pm afternoon heat index for 2045-2049 and 2095-2099 periods compared to the 2006-2010 baseline.

Although multi-model high resolution ensembles were not used in this study due to computational cost, changes in internal model variability across time slices and emissions scenarios is explored. Sources of uncertainty in urban modeling may include:

- Representation of urban environment: Although this study uses relatively high-resolution urban canopy parameters, building-atmosphere interactions are heavily parameterized, depending on values averaged over grid points.
- Limited domain size: Due to computational limitations, high resolution urban climate models run on a relatively small domain. Local conditions, in particular heat waves, are

This article is protected by copyright. All rights reserved.

impacted by large scale synoptic processes that may occur thousands of miles away from New York City. Any uncertainties in the input model will be carried over in boundary and initial conditions used in these simulations.

Appendix 2.E. Methods of extreme rainfall analyses.

Table 2.E.1 summarizes the results of the extratropical and tropical cyclone associated analysis. If neither type of cyclone was associated with the precipitation event, the event is labeled non-cyclone. In addition to identifying the total number of cyclone-associated events, we calculate the percent of cyclones that cause extremes. To do this, we divide the number of cyclones associated with a precipitation extreme by the total number of cyclones that pass within 500 km of New York City. For extratropical cyclones, 7.5% of the storms caused a precipitation extreme. For tropical cyclones, the number is much higher, at 30%. This probabilistic calculation cannot be made for non-cyclones, because the storm-type for those events is not known. At least some of those events are most likely associated with are quasi-linear convective systems (Lombardo and Colle 2012), which are sometimes grouped with frontal systems (Kunkel et al. 2011). The dominant cause of extreme daily rainfall events for all airport stations out of these storm types is extratropical cyclones.

Table 2.E.1. Association of daily precipitation extremes at New York City airports from 1979-2016. When 3 values are given, the first is the number of isolated cyclones, the second is the number of extratropical plus tropical cyclones that occurred, the final number is the percentage of cyclone that pass within 500 km of New York City that caused extreme precipitation at the given station.

Storm Type	JFK Airport Station	LaGuardia Airport Station	Newark Airport Station
Extratropical Cyclones	92, 4, 7.4%	92, 3, 7.3%	96, 5, 7.9%
Tropical Cyclone	19, 4, 30.3%	17, 3, 27%	13, 5, 24%
Non-cyclone	23	26	24

Radar was processed with the Hydro-NEXRAD algorithms (Seo et al., 2011) and corrected with a daily multiplicative bias (as in Smith et al. 2012) using rain gauges from the National Oceanic and Atmospheric Administration Meteorological Assimilation Data Ingest system (NOAA MADIS, https://madis.ncep.noaa.gov).

Methods for determining trends in extreme rainfall and proxy-stream flash flooding included the nonparametric Pettitt Test (Pettitt 1979), nonparametric Mann-Kendall Test

This article is protected by copyright. All rights reserved.

Author Manuscript

(Mann 1945, Kendall 1975), and Sen's Slope (Sen 1968). Complete results from these analyses are shown in Tables 2.E.2 and 2.E.3 below.

Table 2.E.2. Statistical analyses of rainfall data in New York City region. Rainfall gauges located at Central Park, LaGuardia airport, Newark airport, and John F. Kennedy airport. Statistics are for 1-hour, 3-hour, 6-hour, and daily annual rainfall maxima. Change points are shown in year and (change in averages), while trends are shown in Sen's Slope.

	Parameter	CP	LGA	EWR	JFK
Hourly Record	Time Period	1948-2013	1948-2013	1948-2013	1969-2013
1 Hour	change point	-	-	1971 (+35%)**	-
	trend	-	-	-	-
3 Hour	change point	1967 (+42%)**	-	-	-
	trend	-	-	0.2 mm/yr**	0.46 mm/yr**
6 Hour	change point	1966 (+34%)**	-	-	-
	trend	-	-	-	-
Daily	change point	1965 (+17%)**	-	1971 (+30%)**	-
	trend	-	-	-	-
Daily Record	Time Period	1869-2017	1940-2017	1893-2017	1959-2017

** indicates a value is significant at a 5% level and * indicates a value is significant at a 10% level.

Table 2.E.3. Statistical analyses of streamflow data in US census New York City urban region. Statistics are for annual peak (maximum) in instantaneous streamflow. Change points are shown in year and (change in averages), while trends are shown in Sen's Slope.

USGS Gauge ID	Location	Timeframe	# Years	Change Point	Trend (cfs/year)	Notes
01374654	Carmel, NY	1996-2012	17	-	-	Regulated flow
01374930	Baldwin Place, NY	1996-2016	21	2011 (-38%)*	-	Occasional regulation
01381400	Morristown, NJ	1996-2015	20	-	-	Diversion upstream

This article is protected by copyright. All rights reserved.

01387450	Suffern, NY	1959-1998 2001-2015	40 15	1967 (+154%)**	-	Well withdrawals upstream
01392210	Passaic, NJ	1977-1999	21	-	-	
01399670	Whitehouse Station, NJ	1978-2015	37	-	14.09*	Occasional regulations and upstream releases
01401650	Belle Mead, NJ	1991-2015	25	-	-	Some irrigation regulation in summer
01403150	Martinsville, NJ	1980-2015	35	-	3.84*	
01403400	Seeley Mills, NJ	1967-2015	49	-	-	Temporarily moved 1969-1979
01403535	Watchung, NJ	1980-2015	36	-	-	
01403540	Watchung, NJ	1973-2015	43	-	-	Occasional regulation, channel modified in 1991 and 1997
01407290	Marlboro, NJ	1980-2015	35	1999 (-25%)*	-	
01407705	Neptune City, NJ	1967-2014	48	-	-	Diversion upstream, a portion is regulated
01407760	Neptune City, NJ	1967-2016	50	-	-7.47**	Upstream diversion water supply and golf courses

**indicates a value is significant at a 5% level and * indicates a value is significant at a 10% level.

Author Manuscript

Appendix 2.F. Methods of Tree-ring Analysis and Drought Analysis

The Pepacton, Canonsville, and Neversink (PCN) reservoir inflows were developed using a Bayesian regression model. Given data from three streamflow gages and eight local tree-ring chronologies (that date back to 1754) as predictor variables, the Bayesian model provides regression equations for each reservoir that are used to hindcast the streamflow. Annual average daily streamflow (June – May) was assumed to follow a lognormal distribution. The Bayesian regression models used to produce this partially pooled reconstruction explain around 60% of the streamflow variance and validate best against withheld data. The posterior probability distributions of the reconstructed combined reservoir inflow from the Bayesian regression model during the period 1754–2000 are shown in Figure 2.13 in the chapter. The record period common to all selected trees determined the time span of the reconstructions. The reconstructions of the combined reservoir inflow are presented as time series composed of boxplots instead of single points, as the reconstructions for each year are estimates of the posterior distribution of the annual

This article is protected by copyright. All rights reserved.

average daily inflow for those years. The boxplots graphically depict those posterior distributions. The record of observed PCN combined inflow data is shown using the 11-year low-pass filtered values (blue color line during the instrumental period (1928 - 2000)). Similar low-pass filtered values are also shown for the median inflows (red color line) during the reconstruction period to visualize the general trend in the data.

Drought Index (Methods)

We developed the drought index to capture the effect of drought over multiple years. The index is based on the sequent peak algorithm. It quantifies the water reservoir drawdown for meeting the demand. The steps for the computation are presented below.

$deficit_t = \max(deficit_{t-1} + D_t - S_t, 0)$, where $deficit_{t=0} = 0$.

$Severity = max_t(deficit_t; t = 1: n\text{-}years)$

$deficit_t$ refers to the accumulated annual deficit, D_t refers to the annual water demand, S_t refers to the annual water supply and n is the total number of years under considerations. The maximum accumulated deficit estimated over the *n-year* period is defined as the *Severity* of the drought. It measures the potential impact of multi-year droughts.

Drought profile based on the reconstructed reservoir inflow data

The demand-specific drought index is applied to the simulations of the reconstructed PCN combined inflows with a demand threshold of 950 MGD of annual average daily flow to develop the long-term drought risk profile. Figure 2.F.1 presents the joint probability distribution of the drought duration and severity as seen from the paleo records. The worst drought event in the instrumental period (the 1960s drought of 6 years and a cumulative deficit of 1000 MGD) is shown as a red circle in the figure. It is evident from the paleo streamflow data that the drought of the record, the 1960s drought, is still an extreme event relative to a long-term drought risk profile. The probability of exceedance of the six-year drought duration is $\mathrm{P}(\mathrm{Duration} > 6) = 0.06$, an approximate average return period of 16 years if drought length is of concern. The probability of exceedance of the 1000 MGD cumulative deficit (drought severity) is $\mathrm{P}(\mathrm{Severity} > 1000\ \mathrm{MGD}) = 0.03$, an approximately average return period of 33 years if drought severity is of concern. However, if combined variables of duration and severity are of interest, the probability of joint exceedance $\mathrm{P}(\mathrm{Duration} > 6 \cap \mathrm{Severity} > 1000) = 0.006$, an approximate average return period of 166 years. Hence, while a drought of a six-year length occurs more frequently than the drought of a 1000 MGD severity, the recurrence of the joint drought as worse as the 1960s is anomalous.

Author Manuscript

This article is protected by copyright. All rights reserved.

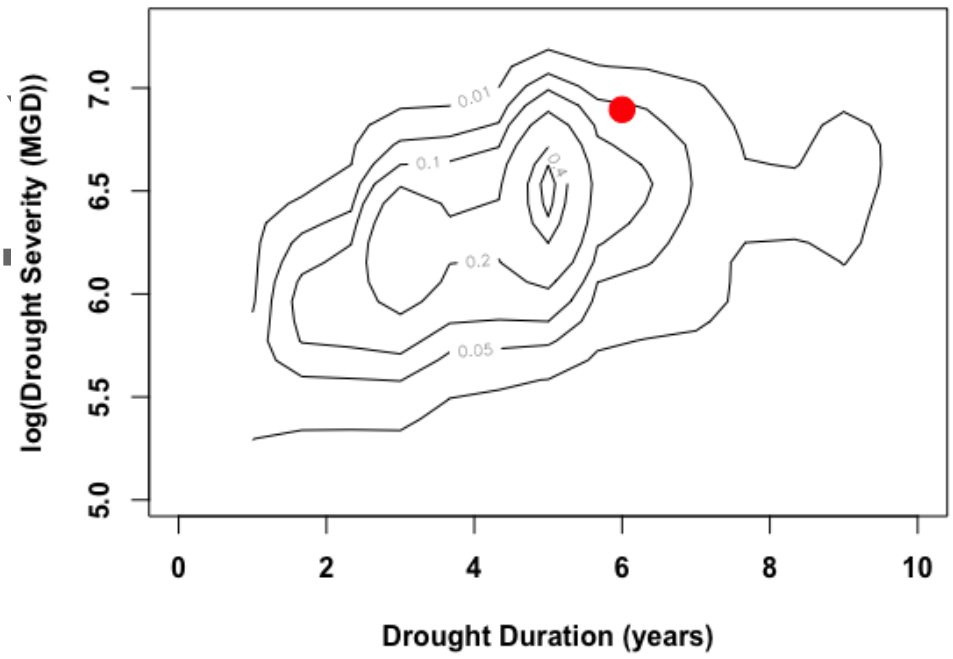

Figure 2.F.1. The joint drought profile for a demand of 950 MGD annual average daily outflow. The contour plot shows the joint probability distribution of drought duration and severity. The drought of the record (1960s drought of 6 years and 1000 MGD cumulative deficit) is shown as a red circle on the contour plot.

Author Manuscript

Drought profile based on the reconstructed reservoir inflow data and changing demand

It is important to note that the drought stress is always relative to the demand of the region. The above analysis is shown for a demand of 950 MGD of annual average daily flow as a benchmark water demand. We have chosen this threshold given this is the average PCN combined reservoir release (including diversions to New York City, conservation, and directed releases) for the last five years. To investigate the effect of water demand on drought stress, we have applied the drought index for four different thresholds, 950 MGD, 1000 MGD, 1050 MGD and 1100 MGD. Any average demand greater than 1100 MGD will exceed the average combined reservoir inflow.

The joint probability distributions of drought duration and drought severity (long-term drought profiles) for various water demand levels is shown in Figure 2.F.2. We observe from these distributions that the drought duration is changing at a rate faster than the drought severity with increasing demand. As the water demand of the region increases, from a long-term planning perspective, the critical metric to focus on will be the length of drought. Drought stress is experienced in terms of its persistence. This can also be seen from Figure

This article is protected by copyright. All rights reserved.

2.F.3, which shows the individual distributions for each of these thresholds along with the drought of the record from the instrumental period.

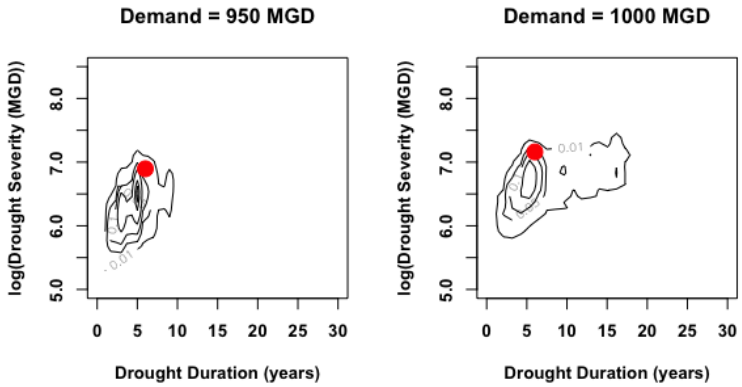

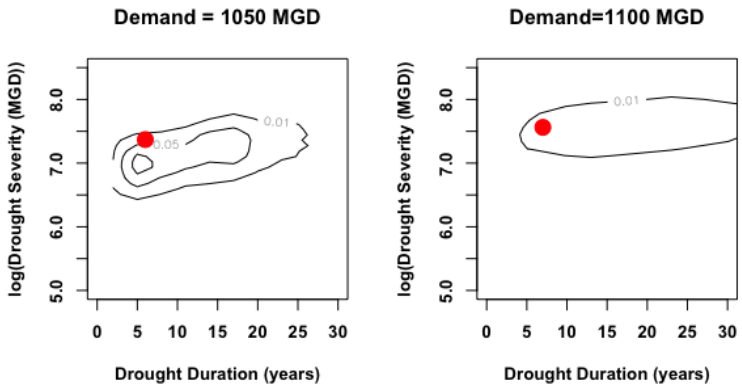

Figure 2.F.2. The joint drought profile for varying demands.

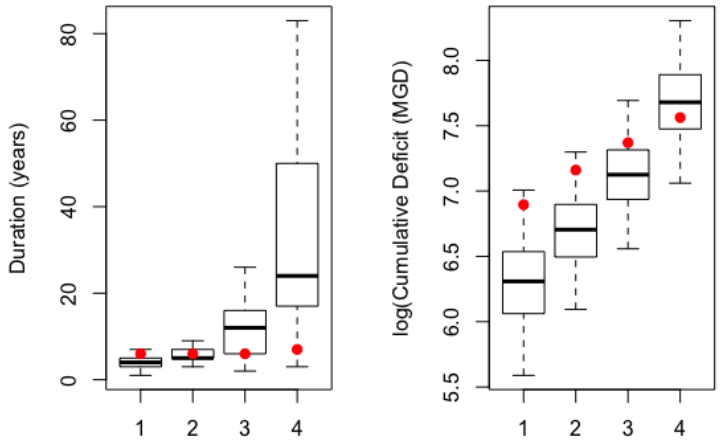

Figure 2.F.3. The distributions of drought duration and severity for varying demands.

This article is protected by copyright. All rights reserved.

Manuscript

The streamflow reconstructions reveal droughts with a longer duration than the duration of the drought seen in the instrumental period (1960s drought). Joint distributions of duration and severity are developed for various demand levels to get a better perspective of the long-term drought profile. Based on a demand level that matches the average reservoir releases for the last five years, the worst drought of the record in the instrumental period is six-year drought with a 1000 MGD cumulative deficit. This event has a joint return period of 166 years when contextualized with the long-term drought profile. However, the drought stress is very sensitive to regional water demand. A marginal increase in the demand from the 950 MGD level will lead to droughts that are longer and more severe, and their joint occurrence becomes more frequent. A comparison of duration vs. severity metrics indicates that the rate of change with respect to demand levels is much faster for the drought duration.

Observed droughts

For the period of 1928-2000, annual average daily inflows and cumulative reservoir deficit was calculated based on a total demand of 950 million gallons per day (MGD) of annual average daily flow (Figure 2.F.4). 950 MGD is approximately the average reservoirs' release for the recent five years.

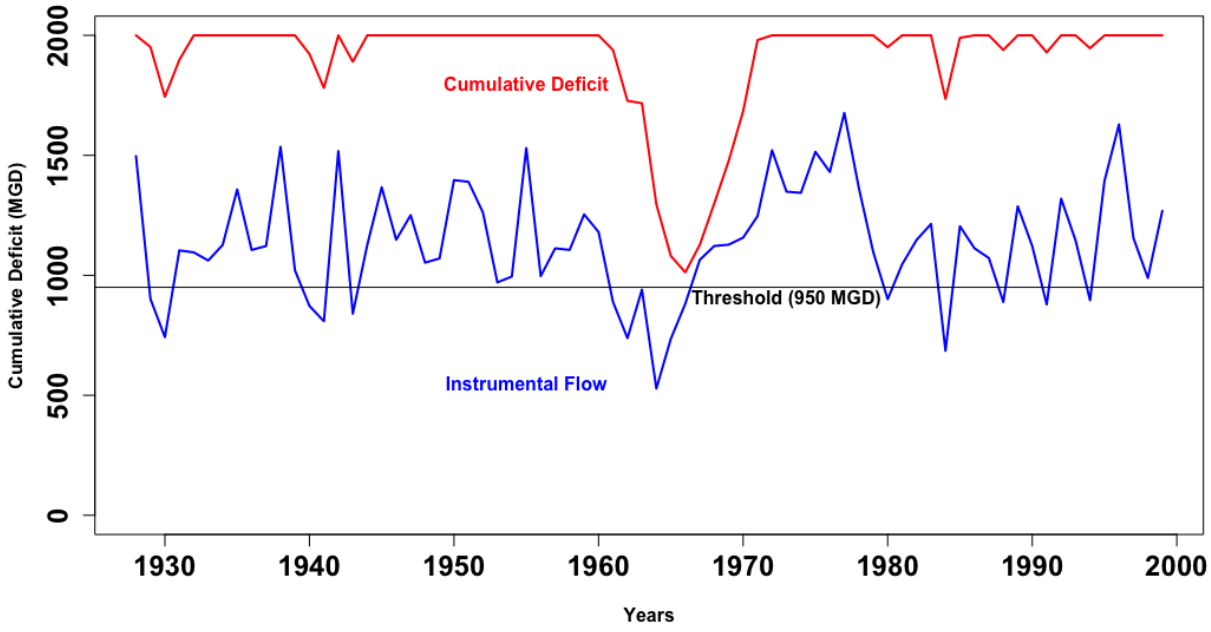

Figure 2.F.4. Annual average daily inflows and cumulative deficit (drawdown) of the combined Pepacton, Canonsville, and Neversink (PCN) reservoir during the instrumental period (1928-2000).

This article is protected by copyright. All rights reserved.

The blue line shows the observed PCN reservoir combined inflow. The red line (inverted) indicates the cumulative deficit.

In the decade of the 1960s, the reservoirs had extensive drawdown, making it the worst drought of the instrumental period. The observed duration of the drought is six years, from 1961 - 1967. The severity of the drought, measured as the cumulative deficit, is approximately 1000 MGD. The recovery period of this drought is five years. While there are other periods with small to moderate droughts, there is no other period in the instrumental record that has a drought as severe as the 1960s drought.

Table 2.F.1 summarizes the individual and joint probability of exceedances and return periods of the drought duration and severity. Evidently, they are very sensitive to the demand. While the droughts stress for a demand level consistent with the water releases for the past five years is moderate, the drought stress is more likely and reoccurs more frequency for a marginal increase in the demand levels.

Table 2.F.1. Summary of the probability of exceedances and the return periods of the droughts for four different demand levels.

		Demand			
		950 MGD $D^* = 6$ $S^* = 1000MGD$	**1000 MGD** $D^* = 6$ $S^* = 1300MGD$	**1050 MGD** $D^* = 6$ $S^* = 1600MGD$	**1100 MGD** $D^* = 7$ $S^* = 1900MGD$
Exceedance Probability	$P(S > S^*)$	0.03	0.04	0.45	0.95
	$P(D > D^* \cap S > S^*)$	0.006	0.028	0.40	0.94
Return Period	Severity	33 yr	25 yr	2.2 yr	1 yr
	Joint	166 yr	36 yr	2.5 yr	1 yr

Author Manuscript

This article is protected by copyright. All rights reserved.